JAERI-M
8060

X-RAY EMISSION FROM HOT PLASMA

January 1979

Satio HAYAKAWA* and Takako KATO**

日本原子力研究所
Japan Atomic Energy Research Institute

JAERI-M 8060

X-RAY EMISSION FROM HOT PLASMA

Satio HAYAKAWA* and Takako KATO**

(Received December 26, 1978)

X-ray emission from hot plasmas is discussed with a critical review of different theories. The results given in the present paper are complementary to those given by Kato in the sense that the present paper is introductory to the paper by Kato. The contents of the present paper are;

1. Introduction
2. Ionization and Recombination Rate Coefficients
3. Relative Abundances of Ions
4. Intensity and Spectra of Radiation
5. Comparison with Earlier Results
6. Emission and Absorption Lines

This work was supported by a research contract "A Study of Elementary Processes (Excitation) of Impurities" of Japan Atomic Energy Research Institute with Nagoya University conducted in fiscal year 1977-8. The present report was received on February 28, 1977 as stipulated in the contract, and is herewith published for its value to scientific community.

*)Department of Physics Nagoya University
**)Institute of Plasma Physics Nagoya University

高温プラズマからのX線輻射

早川　幸男＊・加藤　隆子＊＊

（1978年12月26日受理）

高温プラズマからのX線輻射について，種々の理論の批判的なreviewをしながら，議論する。この論文に示された結果は，加藤（1978）の論文に示されたものの導入部に相当し，相補的な関係がある。

内容は，次のようである。

諸論，電離と再結合係数，イオンの相対素成，輻射の強度とスペクトル，他の結果との比較，線スペクトルの輻射と吸収。

＊）名古屋大学理学部物理

＊＊）名古屋大学プラズマ研究所

本研究は日本原子力研究所が昭和52年度名古屋大学と締結した委託調査「不純物の素過程（励起）」によって実施したものであり本報告書は契約によって定められた通り昭和53年2月28日に納入された。ここに，その科学的価値を考慮して公刊するものである。

Content

1. Introduction

Physical properties of a hot plasma are obtained by observing X-rays emitted therefrom. For example, the electron temperature is derived from the spectra of continuum and lines, and the abundances of ions are obtained from the intensities of characteristic lines. A number of articles have been published to discuss X-ray emission from hot plasma, and the results are applied to derive properties of the solar corona, celestial X-ray sources and laboratory plasmas.

The present article reviews elementary processes relevant to X-ray emission and presents results useful for analyzing observed data. We restrict ourselves to thin plasmas, in which the absorption and scattering of X-rays are negligible except for some resonance lines. We are concerned with practical applications, so that the results expected with detectors of current use are presented.

The present work is based on a lecture note prepared by one of the authors (S.H.) for a summer school of plasma physics in 1969, on a manuscript of his book in preparation, on an article by Kato (1976)[1] and on our interpretation of rocket observations of the diffuse component of cosmic soft X-rays (Hayakawa et al. 1977[2],[3]). The present article is complementary to a recent review by one of us (Kato 1978),[4] but contains overlapping parts for completeness. The readers may get an overview and qualitative understanding from this article, and will obtain quantitative detail from Kato (1978).[4]

2. Ionization and Recombination Rate Coefficients

2.1. General Considerations

The collision of electrons of density n_e with ions of charge z and density n_z produces ions of charge $z+1$ at a rate $C_z n_e n_z$ per unit volume. The ion of charge $z+1$ comes back to ion z by capturing an electron at a rate of $\alpha_{z+1} n_e n_{z+1}$ per volume. C_z and α_z are called the ionization and recombination coefficients, respectively. Hence the ion density charges as

1. Introduction

Physical properties of a hot plasma are obtained by observing X-rays emitted therefrom. For example, the electron temperature is derived from the spectra of continuum and lines, and the abundances of ions are obtained from the intensities of characteristic lines. A number of articles have been published to discuss X-ray emission from hot plasma, and the results are applied to derive properties of the solar corona, celestial X-ray sources and laboratory plasmas.

The present article reviews elementary processes relevant to X-ray emission and presents results useful for analyzing observed data. We restrict ourselves to thin plasmas, in which the absorption and scattering of X-rays are negligible except for some resonance lines. We are concerned with practical applications, so that the results expected with detectors of current use are presented.

The present work is based on a lecture note prepared by one of the authors (S.H.) for a summer school of plasma physics in 1969, on a manuscript of his book in preparation, on an article by Kato (1976)[1] and on our interpretation of rocket observations of the diffuse component of cosmic soft X-rays (Hayakawa et al. 1977[2],[3]). The present article is complementary to a recent review by one of us (Kato 1978),[4] but contains overlapping parts for completeness. The readers may get an overview and qualitative understanding from this article, and will obtain quantitative detail from Kato (1978).[4]

2. Ionization and Recombination Rate Coefficients

2.1. General Considerations

The collision of electrons of density n_e with ions of charge z and density n_z produces ions of charge z+1 at a rate $C_z n_e n_z$ per unit volume. The ion of charge z+1 comes back to ion z by capturing an electron at a rate of $\alpha_{z+1} n_e n_{z+1}$ per volume. C_z and α_z are called the ionization and recombination coefficients, respectively. Hence the ion density charges as

$$\frac{dn_z}{dt} = [C_{z-1} n_{z-1} n_e - \alpha_z n_z n_e] - [C_z n_z n_e - \alpha_{z+1} n_{z+1} n_e] \ . \qquad (2.1)$$

Here we have neglected processes of changing two or more units of charge, since the probabilities for such processes are small in the plasmas of interest.

In cosmic X-ray sources electrons are mostly produced from hydrogen and helium whose abundances are far greater than the abundances of heavier elements. In laboratory plasmas for controlled nuclear fusion heavy ions of interest are admixed as impurities. In both cases the electron density remains practically unchanged in the course of the ionization of and the recombination of heavy ions. Hence equation (2.1) is reduced to

$$\frac{dn_z}{d\tau} = [C_{z-1} n_{z-1} - \alpha_z n_z] - [C_z n_z - \alpha_{z+1} n_{z+1}] \ . \qquad (2.1')$$

with the reduced time

$$\tau = n_e t \ . \qquad (2.2)$$

In non-steady processes the results are represented as functions of reduced time τ.

If a term in the right hand side of equation (2.1') is smaller than the reciprocal time scale under consideration, for instance,

$$C_z n_z t \ll 1 \text{ or } \alpha_z n_z t \ll 1 \ , \qquad (2.3)$$

the relative ion abundances do not yet reach an equilibrium value but are changing with time. In this case the ionization state is said to be non-steady.

After sufficiently long time the ionization state becomes steady, and each square bracket of equation (2.1') vanishes. Then the relative ion abundances are given by

$$n_z / n_{z+1} = \alpha_{z+1} / C_z \ . \qquad (2.4)$$

Since C_z and α_z are functions of electron temperature, the ion abundances are determined by a given electron temperature. A plasma in a steady

ionization state at a constant temperature is said to be in ionization equilibrium.

Ionization and recombination are not always dictated by binary collisions alone, as expressed by equation (2.1). In the circumstellar matter of a strong X-ray source and in the gas blanket of a hot laboratory plasma, photoionization may be more efficient than collisional ionization. If the electron density is higher than $10^{14}\ Z^8\ cm^{-3}$, two electron recombination is no longer negligible. However, we do not consider processes other than the binary collisions in the present paper. Among binary processes we neglect the charge exchange collision between two ions.

We further restrict ourselves to the case where the velocity distribution of electrons is isotropic and Maxwellian. However, we do not always assume a thermal equilibrium between electrons and ions. The result does not directly depend on the ion temperature, although heating of electrons by hot ions is considered for the case of shock heated plasmas.

There are many simplifying assumptions other than those mentioned above. Hence the applicability of our results is limited to idealized cases. Nevertheless, our results are useful for understanding essential properties of those plasmas which are found in many X-ray sources and various laboratory plasmas.

2.2 Ionization

If an electron of energy higher than the ionization energy collides with an ion, the ion may be ionized by ejecting a bound electron. If the electron is ejected by a single step, the process is called direct ionization. There is a process, in which an inner shell electron is excited to a higher bound state and then deexcited by ejecting an electron in a way similar to the Auger effect. This is called autoionization. If an inner electron is directly ionized, the Auger effect results in the loss of two electrons. This process is not included in equation (2.1), since its contribution to ionization is not important for Maxwellian electrons.

Several expressions for the direct ionization cross section have been proposed, and they are compared with each other and with an experimental result for the ionization of OIII (Aitken and Harrison 1971),[5]

as reviewed by Kato (1977).[6] The cross section by Seaton (1964)[7] agrees best with the experiment for OIII at energies below 100 eV, whereas that by Lotz (1967,[8] 1968[9]) fits well with the experiment thereabove. This is because Seaton's formula is to simulate the cross section for low z in the energy range $E < 2I$ where I is the ionization energy, and because Lotz' formula underestimates the effect of inner shell ionization for $z \leq 4$ and $E < 2I$. The difference between them is within factor 2 for $E < 2I$, which is comparable to the contribution of processes we have neglected.

For a thin plasma of high temperatures we use Lotz' cross section, since it is applicable over a wide range of energy. The direct ionization rate with Lotz' cross section is represented by

$$C_d = 6.7 \times 10^{-7} \sum_{j=1}^{N} \frac{a_j \xi_j}{T_e^{3/2}} \left[\frac{1}{x_j} Ei(x_j) - \frac{b_j \exp c_j}{x_j + c_j} Ei(x_j + c_j)\right] \text{ cm}^3\text{s}^{-1} , \qquad (2.5)$$

where T_e is the electron temperature in eV, $x_j = I_j/T_e$, I_j being the ionization of the j-th subshell, $Ei(x) = \int_x^\infty dt\, e^{-t}/t$, ξ_j is the number of electrons in the j-th subshell, and a_j, b_j and c_j are parameters of order unity. The values of I_j, a_j, b_j and c_j are tabulated by Lotz (1967,[8] 1968[9]) with N = 1 for H and He, N = 2 for Li through Ar and N = 3 for K through Zn. Asymptotic expressions for low and high temperature limits are

$$C_d \simeq 3.0 \times 10^{-6} \xi_1 \left(\frac{a_1}{4.5}\right)(1 - b_1) \frac{T_e^{1/2}}{I_1^2} e^{-I_1/T_e} \text{ cm}^3\text{s}^{-1}$$

$$\text{for } T_e \ll I_1 , \qquad (2.5a)$$

$$C_d \simeq 3.0 \times 10^{-6} \bar{\xi} \left(\frac{\bar{a}}{4.5}\right) T_e^{-1/2} \bar{I}^{-1} \left(\ln \frac{T_e}{\bar{I}} - 0.577\right) \text{ cm}^3\text{s}^{-1}$$

$$\text{for } T_e \gg I_1 , \qquad (2.5b)$$

where the bar represents the weighted mean over shells. Since $x\, Ei(x) < \exp(-x)$, the expression (2.5a) gives an overestimate of the expression (2.5).

Equation (2.5a) can be compared with the direct ionization rate given by Seaton (1964).[7]

$$C_d = 2.15 \times 10^{-6}\ T_e^{1/2} \sum_j \frac{\xi_j}{I_j^2} \exp(-\frac{I_j}{T_e})\ \mathrm{cm}^3\mathrm{s}^{-1} \quad . \tag{2.6}$$

Since an estimated error of Lotz' is +40, -30 %, the difference between Lotz' and Seaton's lies within the error for $T_e < I_1$. Hence no radical difference is expected between equilibrium abundances calculated with these two ionization coefficients, on account of that an equilibrium is attained for $T_e < I_1$.

In connection with iron line emission from the solar corona, the ionization rate by autoionization has been found important for some ions. Jordan (1969[10]) has proposed an empirical formula for the rate coefficient of autoionization,

$$C_a = 3.2 \times 10^{-6}\ fW^{-1}T_e^{-1/2} \exp(-W/T_e)\ \mathrm{cm}^3\mathrm{s}^{-1} \tag{2.7}$$

with

$$\begin{aligned}
&f = 0.70\ \xi\ , \quad && W = I_2 - I_1 && \text{for } I_2 > 2I_1\ ,\\
&f = 0.13\ \xi\ , \quad && W = I_1 && \text{for } 2I_1 > I_2 > 1.56\ I_1\ ,\\
&f = 0.049\ \xi\ , \quad && W = I_1 && \text{for } 1.56I_1 > I_2 > 1.41I_1\ ,\\
&f = 0.023\ \xi\ , \quad && W = I_1 && \text{for } 1.41I_1 > I_2\ ,
\end{aligned}$$

where ξ is the number of electrons in the shell from which the excitation takes place. Comparison of equation (2.7) with equation (2.6) demonstrates the importance of the autoionization process for $\xi > \xi_1$; the number of electrons in the inner shell is larger than that of outer electron.

2.3. Recombination

In a thin plasma recombination takes place through two processes. One is the radiative transition from continuum to a bound level, and the other is the non-radiative capture associated with excitation of a bound electron to an excited level. They are called radiative recombination and dielectronic recombination, respectively. Since few direct

experimental data of the electron capture cross sections are available, we have to rely on the theory of recombination which has been worked out for hydrogenic ions.

The radiative recombination coefficient to all bound levels is given by Seaton (1959[11]) for hydrogenic ions as

$$\alpha_r(x^{z+1} \to x^z) = 1.9 \times 10^{-13}(z+1)^2 \, T_e^{-1/2} \, F(I_z/T_e) \ \mathrm{cm^3 s^{-1}} \ , \qquad (2.8)$$

where I_z is the ionization energy of the ion formed by recombination. The function $F(I_z/T_e)$ is approximately expressed as

$$F(u) \simeq 0.9 \, u^{0.3} \quad \text{for} \quad 0.5 < u \leq 50 \ , \qquad (2.9)$$

the slope gradually decreasing as u increases. Jordan (1969) has assumed $F(u) \simeq 0.6 \, u^{0.5}$ for small u and a constant value of F(u) for large u. This is not essentially different from the approximation given by equation (2.9). If we substitute equation (2.9) in equation (2.8), we obtain

$$\alpha_r = 3.8 \times 10^{-13} \, z^{2.6} \, T_e^{-0.8} \ . \qquad (2.8')$$

This is in qualitative agreement with the numerical results obtained for individual ions by Aldrovandi and Péquignot (1973,[12] 1974[13]), who calculated the recombination rates to excited levels with the hydrogenic approximation and the rate to the ground level with the photoionization cross section. Because the u-dependence of F(u) deviates from the approximate expression in equation (2.9), equation (2.8') gives an overestimate for small u and an underestimate for $1 < u < 5$. In addition, more accurate values for individual ions scatter about the simplified expression (2.8') by 30 % or so.

For quantitative use we recommend the formula

$$\alpha_r = A_r T_e^{-\eta_r} \ , \qquad (2.8')$$

proposed by Aldrovandi and Péquignot (1973,[12] 1974[13]). The numerical values of A_r and η_r along with the values of parameters for dielectronic recombination are reproduced in Table 3 of Kato (1978).[4]

The dielectronic recombination coefficient is given by Burgess

(1965)[14] as

$$\alpha_d = 2.4 \times 10^{-9}\, B(z) T_e^{-3/2} \sum_j f_{ij} A(q_{ij}) \exp(-E_{ij}/T_e)\ \mathrm{cm^3 s^{-1}} \quad . \quad (2.10)$$

where f_{ij} is the oscillator strength, $q_{ij} = (z+1)(n_i^{-2} - n_j^{-2})$, $E_{ij} = I_z(n_i^{-2} - n_j^{-2})/[1 + 0.015z^3/(z+1)^2]$, and

$$A(q) = q^{1/2}\,(1 + 0.105q + 0.015q^2) \quad \text{for} \quad q > 0.05 \ ,$$

$$B(z) = z^{1/2}\,(z+1)^{5/2}\,(z^2 + 13.4)^{-1/2} \quad \text{for} \quad z \leq 20 \ .$$

In the summation over j the terms representing the transitions to lower energy states are important. Aldrovandi and Péquignot (1973)[12] have found a simple expression

$$\alpha_d = A_d T_e^{-3/2} \exp(-W_1/T_e)[1 + B_d \exp(-W_2/T_e)] \ , \quad (2.11)$$

whose accuracy compared with numerical results is better than 10 % for most ions and not worse than 25 % for others over the temperature range $T_{max} > T > T_{crit}$. The numerical values of A_d, B_d, W, and W_2 are also given in Table 3 of Kato (1978).[4] The numerical values of A_d and W_1 are approximately expressed for respective isoelectronic sequences as

$$A_d = A_o\,(z+1)^{\xi} \ , \quad (2.12a)$$

$$W_1 = W_o\,(Z + K)^{\xi} \ . \quad (2.12b)$$

The values of A_o, ξ, W_o, k and ξ are given in Table 1. No simple expressions are found for B_d and W_2. The expressions (2.12) and the numerical values in Table 1 may serve for obtaining approximate values of the recombination coefficient, but the readers are recommended to use Table 3 of Kato (1978)[4] for quantitative use.

As readily seen from the numerical values, the dielectronic recombination rate is relatively small for ions with K-electrons and the closed shell compared with ions with partly filled L or M shell, although this is comparable to or greater than the radiative recombination rate for $T_e \sim \frac{1}{2} I_z$.

In calculating the dielectronic recombination coefficient (2.10),

the Auger effect associated with deexcitation is taken into account only for transitions into the ground level. It has been pointed out by Jacobs et al (1977),[15],[16] however, that the Auger effect is not always negligible even for transitions to excited levels, such as for the 3d-2p transition of FeXVII. Hence the dielectronic recombination coefficient is smaller than that given by equation (2.10) or (2.11).

2.4 Density Dependent Effects

If the electron density is high, the lifetime of a highly excited ion for collisional ionization becomes shorter than that of radiative deexcitation. Hence such levels are regarded as belonging to continuum. The principal quantum numbers of such levels are greater than n_t, which is given by (Griem 1964)[17]

$$n_t \simeq 1.26 \times 10^2 \ (z^7/n_e)^{2/17} \ (T_e/z^2 I_H)^{1/17} \ \exp(4z^2 I_H/17 n_t \ ^3T_e) \ . \tag{2.13}$$

The value of n_t depends only weakly on $z^2 I_H/T_e$, where I_H is the ionization potential of HI, and decreases in proportion to $(z^7/n_e)^{2/17}$. The excitation energy of the level n_t is given by

$$I_t \simeq 1.3 \times 10^{-4} \ (I_z/T_e)^{1/7} \ n_e^{2/7} \ \text{eV} \ . \tag{2.14}$$

The rate for collisional ionization via such bound levels is expressed as (Wilson 1964,[18] 1967[19])

$$C_b = 4.5 \times 10^{-7} \ z^{-2} n_t^{-2} T_e^{-1/2} \exp \{-(I_z + I_t)/T_e\} \ \text{cm}^3\text{s}^{-1} \ . \tag{2.15}$$

The rate of stepwise ionization caused by excitation to the levels higher than n_t is much smaller than the direct ionization rate unless $n_t \lesssim 10$, so that this process can be neglected for highly ionized heavy ions in an optically thin plasma.

Recombination processes are also modified by the presence of these bound states. The summation over bound levels for the dielectronic recombination rate in equation (2.10) should be cut off at n_t. This reduces the value of α_d. In stead, radiative decay from these bound levels to lower levels should be regarded as recombination.

The recombination rate for this process is given by (Wilson 1967)[19]

$$\alpha_b = 0.97 \times 10^{-12}\ z^4 n_t^{-1} T_e^{-3/2} \exp\ (I_t/T_e)\ \mathrm{cm}^3\mathrm{s}^{-1}\ . \qquad (2.16)$$

This is also negligble compared with others, unless $n_t \lesssim 10$ and the principal quantum number of the ground level is large. Moreover, the contribution of α_b is partly compensated by the reduction of α_d.

If the electron density is still higher, two-electron recombination may have to be taken into account. The rate coefficients are given for the respective cases, where one of the electrons is bound in a level of $n \geq n_t$ and where both two are free, as (Wilson 1967).[19]

$$\alpha_{b2} = 1.5 \times 10^{-28}\ n_e z^{-2} n_t^{-2} T_e^{-2} \exp(I_t/T_e)\ \mathrm{cm}^3\mathrm{s}^{-1}\ , \qquad (2.17a)$$

$$\alpha_{c2} = 4.6 \times 10^{-29}\ n_e z^{-2} T_e^{-2}\ \mathrm{cm}^3\mathrm{s}^{-1}\ . \qquad (2.17b)$$

Hence these processes are import and at very high densities and low temperatures.

In the present paper we neglect all these effects, as we are concerned with thin, hot plasmas. However, we add this subsection in order to give the limit of applicability of our results.

2.5. Numerical Examples

The numerical values of C_d, C_a, α_r and α_d are given against T_e for oxygen and iron in figure 1, as these two elements are important for cosmic X-ray sources as well as contaminations in laboratory plasmas.

3. Relative Abundances of Ions

3.1. General Considerations

Figure 1 indicates that $C = \alpha$ reaches at $T_e < I$, unless z is very large. If the temperature deviates from an equilibrium temperature by ΔT_e, the time to reach a new equilibrium is on the order of $(I\Delta T_e/T_e^2)/Cn_e$. If the time scale of temperature fluctuations is shorter than this,

The recombination rate for this process is given by (Wilson 1967)[19]

$$\alpha_b = 0.97 \times 10^{-12}\ z^4 n_t^{-1} T_e^{-3/2} \exp\ (I_t/T_e)\ \mathrm{cm}^3\mathrm{s}^{-1}\ . \qquad (2.16)$$

This is also negligble compared with others, unless $n_t \lesssim 10$ and the principal quantum number of the ground level is large. Moreover, the contribution of α_b is partly compensated by the reduction of α_d.

If the electron density is still higher, two-electron recombination may have to be taken into account. The rate coefficients are given for the respective cases, where one of the electrons is bound in a level of $n \geq n_t$ and where both two are free, as (Wilson 1967).[19]

$$\alpha_{b2} = 1.5 \times 10^{-28}\ n_e z^{-2} n_t^{-2} T_e^{-2} \exp(I_t/T_e)\ \mathrm{cm}^3\mathrm{s}^{-1}\ , \qquad (2.17a)$$

$$\alpha_{c2} = 4.6 \times 10^{-29}\ n_e z^{-2} T_e^{-2}\ \mathrm{cm}^3\mathrm{s}^{-1}\ . \qquad (2.17b)$$

Hence these processes are import and at very high densities and low temperatures.

In the present paper we neglect all these effects, as we are concerned with thin, hot plasmas. However, we add this subsection in order to give the limit of applicability of our results.

2.5. Numerical Examples

The numerical values of C_d, C_a, α_r and α_d are given against T_e for oxygen and iron in figure 1, as these two elements are important for cosmic X-ray sources as well as contaminations in laboratory plasmas.

3. Relative Abundances of Ions

3.1. General Considerations

Figure 1 indicates that $C = \alpha$ reaches at $T_e < I$, unless z is very large. If the temperature deviates from an equilibrium temperature by ΔT_e, the time to reach a new equilibrium is on the order of $(I\Delta T_e/T_e^2)/Cn_e$. If the time scale of temperature fluctuations is shorter than this,

the ion abundances do not appreciably fluctuate. This means that a change of ion abundances is generally behind a change of temperature. The time delay of ionization or recombination with respect to a temperature change is important, if a plasma is rapidly heated or cooled.

For rapid heating ionization takes place with a time scale of $1/Cn_e$. Since the ionization drops by a large factor when the next shell ionization starts, ions with a closed shell are abundant for a considerable time interval.

If a plasma of high temperature is rapidly cooled, recombination takes place with a time scale of $1/\alpha n_e$. Since the dielectronic recombination is relatively low for closed shell ions, they are abundant for a relatively long time interval.

A plasma is called ionizing or recombining, depending on whether $C_z n_z >> \alpha_{z+1} n_{z+1}$ or $\alpha_{z+1} n_{z+1} >> C_z n_z$. Such cases are commonly observed for a tenuous plasma, since the rates of ionization and recombination are proportional to the electron density n_e. Even for a dense plasma these states are observed if heating and cooling are very rapid as in the case of a laser heated plasma.

3.2. Ionizing Plasmas

A plasma is ionizing to the ionization state z, if $C_z n_z < \alpha_{z+1} n_{z+1}$ and $\alpha_z n_e t < 1$. Since $C_{z-1} > C_z$ and $\alpha_{z-1} < \alpha_z$ in most cases, the recombination terms in equation (2.1) can be neglected. Ions are successively ionized until either of the above conditions ceases to hold or ions are completely ionized.

If the temperature is kept constant, an analytic solution of equation (2.1) is obtainable. A numerical example is given in figure 2.

The general behaviour of ionization may be understood in the following way. The time scale for increasing a degree of ionization is $1/C_z n_e$. The maximum abundances for respective degrees of ionization are proportional to $1/C_z$. The time for ions of charge y to be transformed to those of z is estimated as

$$t_i \simeq \sum_{k=y}^{z-1} (1/C_k n_e) \quad . \tag{3.1}$$

The following remark may be worth while for a dense plasma. If n_t given in equation (2.16) is small, collisions which would otherwise lead

to excitation followed by radiation are regarded as ionization. Hence line emission hardly takes place in a dense, ionizing plasma of very small n_t.

3.3. Recombining Plasmas

In the opposite case we can neglect the ionization terms, and the degree of ionization decreases with the time scale of $1/\alpha n_e$. An example is given for constant temperatures in figure 2(b).

In a recombining plasma the relative intensities of lines are dictated by the probabilities of recombination to respective levels and of cascade transitions. In the case of high densities, however, two electron recombination dominates over other recombination processes, and the radiation power is relatively weak in comparison with the recombination rate in continuum.

3.4. Ionization Equilibria

Ion abundances in ionizing and recombining plasmas tend constant values as time goes on. The equilibrium abundances are calculated from a set of equations (2.4). The result given for abundant elements by Jordan (1969)[10] has been widely used. She employed the rate coefficients mainly derived by Seaton (1959,[11] 1964[7]) with appropriate approximations as described before and took into account the density effects for the solar corona. The results should be essentially the same as those derived with the rate coefficients recommended in the present paper because of rather small differences between hers and ours, except for the dielectronic recombination coefficient. In figure 3 we compare the equilibrium abundances of Fe ions given by Jordan (1969)[10] with those by Jacobs et al (1977)[15][16] who took into account autoionization associated with transitions to excited states. In general the maximum abundance of an ion appears at a lower temperature in the latter work because of a smaller recombination coefficient.

Since the relative ion abundances are sensitive to temperature, the electron temperature can be accurately obtained by observing X-ray lines of known oscillator strengths characteristic to respective ions, if the ionization equilibrium is found to hold. In practice, however, it is not always easy to know whether a plasma is in ionization equilibrium or not.

4. Intensity and Spectrum of Radiation

4.1. Emission Processes

When an electron collides with an ion, radiation can be emitted by free-free, free-bound and bound-bound transitions. Free-free emission is also called bremsstrahlung and is associated with Coulomb scattering of an electron to lower free states. If the velocity distribution of electrons is Maxwellian, this is called thermal bremsstrahlung. Free-bound emission is also called recombination radiation. These two processes give a continuous spectrum, whereas bound-bound emission gives a line spectrum except for two-photon emission associated most significantly with the 2s-1s transition, for which one-photon emission is forbidden.

The spectrum of thermal bremsstrahlung spreads over the energy range $\lesssim T_e$, whereas the others give radiation in the energy range around T_e from ions with ionization energies comparable to T_e. In a hydrogen plasma a contaminating heavy element with atomic abundance 10^{-5} times the hydrogen abundance may emit lines and recombination continua as strong as thermal bremsstrahlung in the temperature range $I_1 < T_e < I_z$, where I_z is the ionization energy of an ion with charge z. In a celestial plasma of normal elemental abundances, therefore, bound-bound emission dominates over others in the temperature range 1 - 10^3 eV, and this may also be the case in most laboratory plasmas.

4.2. Thermal Bremsstrahlung

The spectrum of thermal bremsstrahlung for a plasma of electron density n_e and ion density n_z is expressed as

$$q_{ff}(E) = 1.0 \times 10^{-13}\ T_e^{-1/2}\ \exp(-E/T_e) \sum_z Z^2\ g_{ff}(E/T_e,\ I_z/T_e)$$

$$n_e n_z\ \text{eV cm}^{-3}\text{s}^{-1}\ \text{eV}^{-1}\ , \qquad (4.1)$$

where E is the photon energy in eV and g_{ff} is the Gaunt factor. The Gaunt factor depends only weakly on I_z/T_e and is approximately expressed as

$$g_{ff}(E/T_e) \simeq \begin{cases} 1.1(E/T_e)^{-0.17} & \text{for } E < T_e \ , \\ 1.0(E/T_e)^{-0.3} & \text{for } E \gtrsim T_e \ . \end{cases} \tag{4.2}$$

The expressions over a wider range of E/T_e and the dependence on I_z/T_e are given in Table 1 of Kato (1978).[4]

The rate of energy generation by free-free emission is obtained as

$$Q_{ff} = \int g_{ff}(E)dE = 1.0 \times 10^{-13} T_e^{1/2} \bar{g}_{ff}(T_e) \sum_z z^2 n_z n_e \quad \text{eV cm}^{-3}\text{s}^{-1} \ , \tag{4.3}$$

where $\bar{g}_{ff}(T_e) \simeq 1.25$ over a wide temperature range.

4.3. Free-Bound Emission

The continuous spectrum of recombination radiation has a lower edge corresponding to the ionization energy of an ion formed by recombination and a width comparable to T_e. For the transition to a bound level of principal quantum number n with $\bar{\xi}_n$ holes, the spectrum of free-bound emission is given by

$$q_{fb,zn}(E) = 2.6 \times 10^{-12} T_e^{-3/2} \sum_z \frac{\bar{\xi}_n}{2n} \left(\frac{I_{zn}}{I_H}\right)^2 \exp\left(\frac{I_{zn} - E}{T_e}\right) n_e n_{z+1} \quad \text{eV cm}^{-3}\text{s}^{-1}\,\text{sV}^{-1} \quad \text{for } E \geq I_{zn} \ , \tag{4.4}$$

where I_{zn} is the ionization energy for the level concerned and I_H is the ionization energy of the hydrogen atom. Since $(\bar{\xi}_n/2n)(I_{zn}/I_n)^2 \sim 1/n^3$, the intensity at $E < I_{zn_o}$ is much smaller than that for transition to the ground state with the principal quantum number n_o. The values of $(\bar{\xi}_n/2n)(I_{zn}/I_H)^2/z^4$ for several transitions are given in Table 2 of Kato (1978).[4]

The rate of energy generation by free-bound emission is

$$Q_{fb} = \sum_z \int dE \sum_n q_{fb,zn}(E) = 2.6 \times 10^{-12} T_e^{-1/2} \sum_z z^4 G_z(n_o) n_e n_{z+1} \quad \text{eV cm}^{-3}\text{s}^{-1} \ , \tag{4.5}$$

where

$$G_z(n_o) = \frac{\bar{\xi} n_o}{2n_o^5} + 1.202 - \sum_{n=1}^{n_o} \frac{1}{n^3} \quad . \tag{4.6}$$

4.4. Bound-Bound Emission

Transition between bound levels takes place in association with recombination and collisional excitation. A photon of energy E_{jk} is emitted by transition from level j to level k, except for the case of multi-photon emission.

The rate equation for ions at level j is written as

$$\frac{dn_j}{dt} = C_j n_o n_e + \alpha_j n_{z+1} n_e - A_j n_j \quad , \tag{4.7}$$

where n_j is the population of ions with charge z at level j, and A_j is the rate of decay from level j. The rate coefficient for recombination to level j, α_j, is given by taking into account the recombination probabilities to higher levels and cascade transitions to level j as well as the direct transition to level j. The rate coefficients for collisional excitation and deexcitation C_j are obtained in a similar way by taking into account transitions from lower and higher levels.

If recombination is dominant, the population n_j increases at a rate of $\alpha_j n_{z+1} n_e$ and reaches the steady state value $\alpha_j n_{z+1} n_e / A_j$ for $t > 1/A_j$. Then the power is given by

$$P_{jk} = \alpha_j n_{z+1} n_e B_{jk} E_{jk} \quad , \tag{4.8}$$

where B_{jk} is the branching ratio for the radiative decay to level k.

Dielectronic recombination may form an doubly excited ion with one of the electrons to lie in an orbit similar to the orbit of an excited ion of charge z. Radiative transition of this electron gives a line close to the corresponding line for the ion of z. The former is called the satellite line with respect to the latter. For example, a H-like ion captures an electron by dielectronic recombination to a 2pnl state, and the energy for 2pnl - 1snl transition is slightly smaller than that for the corresponding transition 2p - 1s for a H-like ion. The relative intensity of a satellite line is sensitive to the electron temperature,

and does not depend on the ion density if the main line is emitted by collisional excitation. Thus the relative intensity is useful to determine the electron temperature. Since the satellite lines are relatively weak in tenuous plasmas, we shall not go further into this problem but merely refer section 4.4 and figure 8 of Kato (1978).[4]

If the ground state is far more highly populated than excited states, as this is the case for tenuous plasmas where recombination term is neglected, we have only to take into account the excitation from the ground level. Ions at level j are depopulated by collisional excitation and deexcitation as well as by radiative transition, but only the last one is of practical importance for tenuous plasmas. In this case, the population n_j increases at a rate of $C_{oj} n_e n_o$ and reaches the steady state value $C_{oj} n_e n_o / A_j$ for $t > 1/A_j$. Hence the line emission power is given by

$$P_{jk} = C_{oj} n_o n_e B_{jk} E_{jk} \quad . \tag{4.9}$$

For K X-ray emission from ions with outer shell electrons, the branching ratio is equal to the K fluorescence yield.

For H-like ions excited to the 2S level two photons are emitted with a continuous spectrum

$$\frac{dP}{dE} = 12 \frac{C_{o2S}}{E_{2S}} n_o n_e \left(\frac{E}{E_{2S}}\right)^2 \left(1 - \frac{E}{E_{2S}}\right) \quad , \tag{4.10}$$

where E_{2S} is the excitation energy to the 2S level.

Various authors have proposed different rate coefficients for collisional excitation as compared by Kato (1977).[6] Among them the formula proposed by Mewe (1972)[20] gives good fit to experiments. For excitation energy E_{jk}

$$C_{jk} = 1.6 \times 10^{-5} \, T_e^{-1/2} \, (f_{jk}/E_{jk}) \, g(E_{jk}/T_e) \ \mathrm{cm^3 s^{-1}} \quad , \tag{4.11}$$

where f_{jk} is the oscillator strength and

$$g(y) = A + (By - Cy^2 + D) \, e^y \, Ei(y) + Cy \quad . \tag{4.12}$$

Here

$$e^y \, Ei(y) = e^y \int_y^\infty \frac{e^{-x}}{x} dx \simeq \ln\left(\frac{y+1}{y}\right) - \frac{0.4}{(y+1)^2} \quad . \tag{4.13}$$

The values of A, B, C and D are listed in Kato (1976,[1] 1977[6]). The numerical values of C_{jk} for low lying allowed levels are significantly greater than those of C_d as given in equation (2.5a) because of $E_{jk} < I_1$ and a greater numerical coefficient for C_{jk}.

4.5. Emission Power

Emission power from a particular ion species is proportional to its density n(Z, z) which should be substituted to n_o in equation (4.9). For the degree of ionization $n(Z, z)/n_Z$ and the relative abundance n_Z/n_H, the electron density is expressed by

$$n_e = \sum_{Z,z} z n(Z,z) = \left\{ 1 + \sum_{Z,z} z \frac{n(Z,z)}{n_Z} \frac{n_Z}{n_H} \right\} n_H \quad , \tag{4.14}$$

where the complete ionization of hydrogen is assumed in the third expression. For celestial objects the contribution of elements heavier than helium to electrons is negligible, and helium is completely ionized in X-ray sources. Then equation (4.14) is reduced to

$$n_e = \{ 1 + 2n(He)/n_H \} \, n_H \quad . \tag{4.14'}$$

Hence equation (4.9) is expressed as

$$P_{jk} = \frac{n_e^2}{[1 + 2n(He)/n_H]} \frac{n(Z,z)}{n_Z} \frac{n_Z}{n_H} C_{oj} B_{jk} E_{jk} \quad . \tag{4.15}$$

4.6. Emission Rates of Selected Lines

The photon emission rates of strong lines collisionally excited are given for selective ions of O, S and Fe in figure 10 of Kato (1978).[4] The temperature dependence is strong, as expected from the factor $\exp(-E/T_e)$.

Under the ionization equilibrium, the emission rate for a given element density is given by the product of the emission rate of a given ion and the fractional abundance of the ion. The emission rates divided by $n_e n_Z$ are given for selected lines of O, S and Fe in figure 4. The abundances of O and S ions are adopted from Jordan (1969),[10] whereas those of Fe ions from Jacobs et al. (1977)[15][16]; the results with Jordan's abundances are compared for FeXIII, FeXIV and FeXVII. The emission rates for the cosmic abundances are given in figure 9 of Kato (1978).[4]

The energy loss rates by line emission of individual elements are given under the equilibrium condition in figure 5. The loss rate of each element shows a few peaks which correspond to respective electron shells. The contributions of strong lines to the loss rate are given for each O, S and Fe in figure 6. In a given temperature range the contribution of a particular shell dominates over others. The radiation loss rate for the cosmic abundances are shown in figure 13(b) of Kato (1978),[4] in which bremsstrahlung and recombination radiation are included. This demonstrates how important the line emission is.

5. Comparison with Earlier Results

5.1. Ion Abundances

X-ray emission from a hot plasma has been most extensively investigated for the application to the solar corona. Jordan (1969)[10] has given the ion abundances for the temperature range 5×10^3 - 10^7 K. The electron density varies, according to her model of the solar corona and chromosphere, from 3.4×10^{11} - 2×10^8 cm^{-3}, so that $n_e T_e = 8 \times 10^{14}$ cm^{-3} K holds over the temperature range 2×10^4 - 5×10^5 K. The ion abundances thus calculated under ionization equilibrium are model dependent, since the density effect is appreciable at high densities and the density is uniquely related to the temperature.

X-ray emission from a hot interstellar plasma is free from the density effect, since the electron density is comparable to or smaller than 1 cm^{-3}. Then the ion abundances are independent of the electron density and depend only on the electron temperature. Numerical results

Under the ionization equilibrium, the emission rate for a given element density is given by the product of the emission rate of a given ion and the fractional abundance of the ion. The emission rates divided by $n_e n_Z$ are given for selected lines of O, S and Fe in figure 4. The abundances of O and S ions are adopted from Jordan (1969),[10] whereas those of Fe ions from Jacobs et al. (1977)[15][16]; the results with Jordan's abundances are compared for FeXIII, FeXIV and FeXVII. The emission rates for the cosmic abundances are given in figure 9 of Kato (1978).[4]

The energy loss rates by line emission of individual elements are given under the equilibrium condition in figure 5. The loss rate of each element shows a few peaks which correspond to respective electron shells. The contributions of strong lines to the loss rate are given for each O, S and Fe in figure 6. In a given temperature range the contribution of a particular shell dominates over others. The radiation loss rate for the cosmic abundances are shown in figure 13(b) of Kato (1978),[4] in which bremsstrahlung and recombination radiation are included. This demonstrates how important the line emission is.

5. Comparison with Earlier Results

5.1. Ion Abundances

X-ray emission from a hot plasma has been most extensively investigated for the application to the solar corona. Jordan (1969)[10] has given the ion abundances for the temperature range 5×10^3 - 10^7 K. The electron density varies, according to her model of the solar corona and chromosphere, from 3.4×10^{11} - 2×10^8 cm^{-3}, so that $n_e T_e = 8 \times 10^{14}$ cm^{-3} K holds over the temperature range 2×10^4 - 5×10^5 K. The ion abundances thus calculated under ionization equilibrium are model dependent, since the density effect is appreciable at high densities and the density is uniquely related to the temperature.

X-ray emission from a hot interstellar plasma is free from the density effect, since the electron density is comparable to or smaller than 1 cm^{-3}. Then the ion abundances are independent of the electron density and depend only on the electron temperature. Numerical results

in the present paper and of Kato (1978)[4] are applied to thin plasmas without the density effect.

The fractional ion abundances in these two cases are compared in figure 7. They are found appreciably different for OIV and FeIX but not for OVII. It should be noted that the density effect depends not only through $n_t \propto z^{12/17}$ as shown in equation (2.13) but also through the temperature dependence of n_e.

Jordan's abundances with the density effect have been adopted by Mewe (1972b,[21] 1975[22]), by Tucker and Koren (1971)[23] and by Kato (1976),[1] whereas Landini and Fossi (1970)[24] have calculated the ion abundances by themselves under the same conditions. Jordan's results in the low density limit simulate the ion abundances in interstellar plasmas and have been adopted by Stern et al (1978)[25] and by Kato (1978).[4] Under the same conditions Raymond and Smith (1977)[26] have calculated the ion abundances using the ionization cross sections calculated by Summers (1974).[27] Since Summer's cross sections are generally smaller than those by Seaton (1959,[11] 1964[7]) and by Lotz (1967,[8] 1968[9]), the abundance maximum is attained by Raymond and Smith (1977)[26] at a higher temperature than that by Jordan. The fractional ion abundances adopted by Kato (1978)[4] and by Raymond and Smith (1977)[26] are compared in figure 8.

For the application to celestial X-ray emission the abundances of elements have to be assumed. The abundances (a) in Table 2 were generally accepted as the solar abundances in the middle 1960's and have been adopted by Landini and Fossi (1970),[24] by Tucker and Koren (1971)[23] and by Kato (1976).[1] Mewe (1972b)[21] also adopted similar abundances. The abundances (b) in Table 2 were compiled as the cosmic abundances by Allen (1973).[28] The Allen abundances have been adopted by Raymond and Smith (1977),[26] by Stern et al (1978)[25] and by Kato (1978).[4]

5.2. Emission Lines

The intensities of emission lines calculated by various authors are considerably different from each other, whereas there is general agreement in the cross section for continuum emission. The numbers of lines and their wavelength ranges adopted by respective authors are tabulated in Table 3 along with the assumptions for calculating ion abundances.

If the same line emission rates were adopted by different authors,

they would give an identical spectrum for the same ion abundances. The spectra obtained by Landini and Fossi (1970),[24] by Tucker and Koren (1971)[23] and by Kato (1976)[1] are compared in figure 9. Landini and Fossi have given a smaller intensity than others, mainly because they have taken too small a number of lines into account; hundreds of weak lines form an apparent continuum level which may, in some wavelength regions at some temperatures, by appreciably higher than the intensity level due to genuine continuous emission. A higher intensity obtained by Tucker and Koren (1971)[23] is attributed to higher values of the collision strengths than adopted by Kato (1976).[1]

Another example of comparison is given for iron lines in figure 10. Jordan's ion abundances in the low density limit are adopted by Mewe (1972b),[21] by Kato (1976)[1] and by Stern et al (1978),[25] whereas different abundances are employed by Raymond and Smith (1977).[26] The temperatures for the maximum emission obtained by Raymond and Smith (1977)[26] are always higher than those by other three, simply because of different ion abundances based on smaller ionization cross sections. Moreover, Raymond and Smith (1977)[26] have assumed the Gaunt factor for $\Delta n = 0$ as equal to that for $\Delta n \neq 0$, namely, $A = 0.15$ in equation (4.12). On the other hand, Kato (1976)[1] has assumed $A = 0.6$ for $\Delta n = 0$. This results in that the X-ray spectrum calculated by Kato[1] is softer than that by Raymond and Smith. Stern et al (1978)[25] have given the emission rates different only by constant factors from Mewe and Kato, but the differences should disappear by correction for their numerical errors. The results by Mewe and by Kato agree with each other. The collision strengths adopted by them for $\Delta n = 0$ agree within a factor of two with experimental results and with more detailed theoretical results, as shown by Kato (1977).[6]

5.3. Recommended References

The above considerations lead us to conclude that the results by Kato (1976,[1] 1978[4]) in the range 1 - 250 Å and by Stern et al (1977)[25] in the range 100 - 1000 Å are recommended to be most reliable, if appropriate correction is made for numerical errors in the latter.

It should, however, be remarked that Jordan's abundances are not always acceptable if the dielectronic recombination rate is greater than the radiative recombination rate. The recombination rates revised by

Jacobs et al (1977)[15][16] should be used for calculating ion abundances, although the revised abundances are to date available only for Si and Fe ions. Another effect which is discarded in the above papers is K X-ray emission associated with K-electron ionization or excitation. Since the K-fluorescence efficiency is large for heavy elements, this process gives a significant contribution to lines from heavy ions such as iron ions. In fact, Itoh (1977)[29] has demonstrated that the intensity of iron K X-rays is comparable to that of resonance lines of FeXXV and FeXXVI in a supernova remnant Cas A.

6. Emission and Absorption Lines

6.1. Plasma Parameters

A hot plasma is characterized by the chemical composition, the ion abundances, the density, the electron and ion temperatures, their spatial variations, and the velocity field. Some of these quantities can be measured in the long wavelength region. For example, the element abundances are quite accurately obtained from the intensities of recombination lines associated with a transition between two levels of high principal quantum numbers, in which the wavelength resolving power is so high that the difference of wavelengths due to different reduced masses can be resolved. This also enables us to obtain the Doppler shifts due to thermal and turbulent motions of ions. Here, however, we discuss measurements to be performed in the X-ray region.

In the X-ray region the spectral resolution available to date is not so good as to resolve the ion velocity smaller than 10^7 cm s^{-1}. Although the turbulent velocity greater than this and the temperature higher than 10^6 K can be measured from the line profile, the observation of X-ray lines may provide information on the ion abundances and the electron temperature.

In a thin plasma the electron temperature is often different from the ion temperature, though the Maxwellian distribution is attainable separately for electrons and ions. The ion abundances are in many cases non-steady. The element abundances, the ion abundances and the electron temperature can be obtained from the relative intensities of relevant

Jacobs et al (1977)[15][16] should be used for calculating ion abundances, although the revised abundances are to date available only for Si and Fe ions. Another effect which is discarded in the above papers is K X-ray emission associated with K-electron ionization or excitation. Since the K-fluorescence efficiency is large for heavy elements, this process gives a significant contribution to lines from heavy ions such as iron ions. In fact, Itoh (1977)[29] has demonstrated that the intensity of iron K X-rays is comparable to that of resonance lines of FeXXV and FeXXVI in a supernova remnant Cas A.

6. Emission and Absorption Lines

6.1. Plasma Parameters

A hot plasma is characterized by the chemical composition, the ion abundances, the density, the electron and ion temperatures, their spatial variations, and the velocity field. Some of these quantities can be measured in the long wavelength region. For example, the element abundances are quite accurately obtained from the intensities of recombination lines associated with a transition between two levels of high principal quantum numbers, in which the wavelength resolving power is so high that the difference of wavelengths due to different reduced masses can be resolved. This also enables us to obtain the Doppler shifts due to thermal and turbulent motions of ions. Here, however, we discuss measurements to be performed in the X-ray region.

In the X-ray region the spectral resolution available to date is not so good as to resolve the ion velocity smaller than 10^7 cm s^{-1}. Although the turbulent velocity greater than this and the temperature higher than 10^6 K can be measured from the line profile, the observation of X-ray lines may provide information on the ion abundances and the electron temperature.

In a thin plasma the electron temperature is often different from the ion temperature, though the Maxwellian distribution is attainable separately for electrons and ions. The ion abundances are in many cases non-steady. The element abundances, the ion abundances and the electron temperature can be obtained from the relative intensities of relevant

lines. If these are known, the absolute intensity gives the emission measure $< n_e^2 >L$, where L is the linear dimension of the plasma along the line of sight. The spatial distribution of the squared density may be obtained from the observations along different lines of sight.

If the density fluctuation is large, the value of $< n_e^2 >^{1/2}$ derived from the emission measure may be considerably different from the average density $< n_e >$. It is often the case that the clumping factor $C \equiv < n_e^2 >^{1/2} / < n_e >$ is appreciably greater than unity. The ion density integrated over the line of sight can be obtained from the absorption spectrum. The absorption line width gives the absorption measure $< n_z >L$.

If both the emission and absorption measures are observed, the density and its fluctuations are obtainable. In practice, the observation of emission with $< n_e n_z >L \gtrsim 10^{15}$ cm^{-5} is easy for the integration time of 1 second, whereas the absorption measure of $< n_z >L \gtrsim 10^{15}$ cm^{-2} is required for conventional detection systems.

6.2. Equivalent Widths of Emission Lines

X-ray spectra to be observed with non-dispersive detectors are discussed by Kato (1978).[4] Most non-dispersive detectors of current use are not suitable for resolving individual lines, even if they are strong. Dispersive systems of high resolution can resolve strong lines which are sparsely populated, but weak lines are so densely populated that they may be observed as a continuum. An emission line can be resolved if its equivalent width is greater than a certain value.

For a line of power P_l the equivalent width in wavelength is defined by

$$W \equiv P_l / (dP_c/d\lambda) \quad , \tag{6.1}$$

where $dP_c/d\lambda$ is the power of continuum per unit wavelength in the region adjacent to the line. Here the continuum includes unresolvable lines. In figure 11 the powers of strong lines from a thin plasma of cosmic abundances are compared with the power of continuum in the wavelength range 1 Å at the wavelength indicated in the parenthesis. Hence the power of a line divided by the power of continuum in figure 11 gives the equivalent width of the line in Å. Strong lines and their wavelengths are listed in Table 4 along with adjacent lines. For different abundances

of elements the power of a line can be obtained by reference to the relative abundances (b) in Table 2 and the abundances concerned.

Let us consider a Bragg crystal spectrometer as a typical example of the dispersive system. If the photon flux of a line $f_1(cm^{-2}s^{-1}sr^{-1})$ is resolved by a crystal of reflectivity R with rocking angle ϕ, the number of photons detected during time t is

$$N_1 = f_1 A\Omega(R/\phi)t \quad , \tag{6.2}$$

where $A\Omega(cm^2sr)$ is the geometrical factor of the detector including its efficiency. The corresponding number of photons for continuum is obtained with use of equation (6.4) as

$$N_c = f_1 (\Delta\lambda/W) A\Omega(R/\phi)t \quad , \tag{6.3}$$

where $\Delta\lambda$ is the larger one of the line width or the minimum wavelength range resolvable. In the presence of detector background of the counting rate C_b, the line can be resolved if

$$N_1 > 3 (N_c + C_b t)^{1/2} \quad , \tag{6.4}$$

or

$$\frac{1}{9} \frac{W}{\Delta\lambda} A\Omega \frac{R}{\phi} t > 1 + (C_b t/N_c) \quad . \tag{6.4'}$$

The quantities other than W are determined by the detector system if the line width is smaller than $\Delta\lambda$, and only W is the quantity representing plasma properties. Hence lines of equivalent widths W smaller than a value given by equation (6.4) should be regarded as forming a continuum.

6.3. Equivalent Widths of Absorption Lines

Allowed lines are strongly scattered with a cross section

$$\sigma(\nu) = \frac{\pi e^2}{mc} \frac{f}{\nu_D} \exp[-(\nu - \nu_o)^2/\nu_D^2] \quad , \tag{6.5}$$

where ν_o is the frequency for the line center and f is the oscillator strength for the transition concerned. The Doppler width ν_D is given by

$$\nu_D = \nu_o \, (v/c) \quad , \tag{6.6}$$

with

$$v^2 = (2kT/M) + v_t^{\,2} \quad , \tag{6.7}$$

where M is the ion mass and v_t is the turbulent velocity. If $v_t^{\,2} << 2kT/M$,

$$\sigma(\nu_o) = 1.2 \times 10^{17} \, \lambda_o \, (A/T_6)^{1/2} \text{ f cm} \quad , \tag{6.8}$$

where $\lambda_o = C/\nu_o$ in Å, A is the ion mass number and T_6 is the kinetic temperature in units of 10^6K. The optical depth at the line center is defined by

$$t_o = \sigma \, (\nu_o) N \quad , \tag{6.9}$$

where N is the column density of ions concerned.

According to the standard theory of the curve of growth, the equivalent width of an absorption line is expressed as

$$\frac{W}{\lambda} = \begin{cases} \pi^{1/2} \left(\frac{v_o}{c}\right) t_o \left(1 - \frac{t_o}{2^{1/2}} + \frac{t_o^{\,3}}{3^{1/2}} \cdots\right) , & t_o << 1 , \\ 2\left(\frac{v_o}{c}\right) (\ln t_o)^{1/2} \left(1 - \frac{\pi^2}{24(\ln t_o)^2} - \frac{7\pi^4}{384(\ln t_o)^4} \cdots\right) , & \\ \frac{\pi^{1/4}}{2} \left(\frac{v_o}{c}\right)^{1/2} \left(\frac{\gamma}{\nu}\right)^{1/2} t_o^{\,1/2} , & \ln t_o >> 1 , \quad |\nu - \nu_o| > \gamma . \end{cases} \tag{6.10}$$

The last expression applies to the damping wing of a strong line with the Lorentzian width γ. In the linear portion of the curve of growth, the equivalent width is generally too small to be observed, and the portion of damping wing is reached only for a few lines. In the logarithmic portion of the curve of growth the value of W/λ is typically on the order of 10^{-3}. However, the plasma of column density as large as $1/\sigma(\nu_o)$ is not easily available.

Note

This report was received on February 28, 1977. The Division of Large Tokamak Development regrets a delay of its publication.

$$\nu_D = \nu_o \, (v/c) \quad , \tag{6.6}$$

with

$$v^2 = (2kT/M) + v_t^{\,2} \quad , \tag{6.7}$$

where M is the ion mass and v_t is the turbulent velocity. If $v_t^{\,2} \ll 2kT/M$,

$$\sigma(\nu_o) = 1.2 \times 10^{17} \, \lambda_o \, (A/T_6)^{1/2} \ \text{f cm} \quad , \tag{6.8}$$

where $\lambda_o = C/\nu_o$ in Å, A is the ion mass number and T_6 is the kinetic temperature in units of 10^6K. The optical depth at the line center is defined by

$$t_o = \sigma \, (\nu_o) N \quad , \tag{6.9}$$

where N is the column density of ions concerned.

According to the standard theory of the curve of growth, the equivalent width of an absorption line is expressed as

$$\frac{W}{\lambda} = \begin{cases} \pi^{1/2} \left(\frac{v_o}{c}\right) t_o \left(1 - \frac{t_o}{2^{1/2}} + \frac{t_o^{\,3}}{3^{1/2}} \cdots\right) , & t_o \ll 1 \ , \\ 2\left(\frac{v_o}{c}\right) (\ln t_o)^{1/2} \left(1 - \frac{\pi^2}{24(\ln t_o)^2} - \frac{7\pi^4}{384(\ln t_o)^4} \cdots\right) , & \\ \frac{\pi^{1/4}}{2} \left(\frac{v_o}{c}\right)^{1/2} \left(\frac{\gamma}{\nu}\right)^{1/2} t_o^{\,1/2} \quad , \quad \ln t_o \gg 1 \ , \quad |\nu - \nu_o| > \gamma \ . & \end{cases} \tag{6.10}$$

The last expression applies to the damping wing of a strong line with the Lorentzian width γ. In the linear portion of the curve of growth, the equivalent width is generally too small to be observed, and the portion of damping wing is reached only for a few lines. In the logarithmic portion of the curve of growth the value of W/λ is typically on the order of 10^{-3}. However, the plasma of column density as large as $1/\sigma(\nu_o)$ is not easily available.

Note

This report was received on February 28, 1977. The Division of Large Tokamak Development regrets a delay of its publication.

References

(1) T. Kato; Ap. J. Suppl. 30 (1976) 397.

(2) S. Hayakawa, T. Kato, F. Nagase, K. Yamashita, and Y. Tanaka; Astron. & Astrophys. 62 (1977a) 21.

(3) S. Hayakawa, T. Kato, F. Nagase, K. Yamashita, T. Murakami, and Y. Tanaka; Ap. J. 213 (1977b) L109.

(4) T. Kato; IPPJ-AM-4 (1978).

(5) K.L. Aitken, and M.F.A. Harrison; J. Phys. B, 4 (1971) 1176.

(6) T. Kato; IPPJ-AM-2 (1977).

(7) M.J. Seaton; Planet Space Sci., 12 (1964) 55.

(8) W. Lotz; Report Institute fur Plasma Physics, IPP 1/62 (1967).

(9) W. Lotz; Report Institute fur Plasma Physics, IPP 1/76 (1968).

(10) C. Jordan; Mon. Not. R. Astr. Soc. 142 (1969) 501.

(11) M.J. Seaton; Mon. Not. R. Astr. Soc., 119 (1959) 81.

(12) S.M.V. Aldrovandi, and D. Péquignot; Astron. & Astrophys. 25 (1973) 137.

(13) S.M.V. Aldrovandi, and D. Péquignot; Astron. & Astrophys. 18 (1974) 21.

(14) A. Burgess; Ap. J. 141 (1965) 1588.

(15) V.L. Jacobs, J. Davis, P.C. Kepple, and M. Blaha; Ap. J. 211 (1977a) 605.

(16) V.L. Jacobs, J. Davis, P.C. Kepple, and M. Blaha; Ap. J. 215 (1977b) 690.

(17) H.R. Griem; "Plasma Spectroscopy" (McGraw-Hill, New York,1964).

(18) R. Wilson; Atomic Collision Processes in Plasmas, AERE-R 4818 (1964).

(19) R. Wilson; Plasmas in Space and in the Laboratory, ESRO SP-20 (1967).

(20) R. Mewe; Astr. & Ap. 20 (1972a) 215.

(21) R. Mewe; Solar Phys. 22 (1972b) 459.

(22) R. Mewe; Solar Phys. 44 (1975) 383.

(23) W.H. Tucker, and M. Koren; Ap. J. 168 (1971) 283.

(24) M. Landini, and B.C. Monsignori Fossi; Astr. & Ap. 6 (1970) 468.

(25) R. Stern, E. Wang, and S. Bowyer; to be published in Ap. J. Suppl. June (1978).

(26) J.C. Raymond, and B.W. Smith; Ap. J. Suppl. 35 (1977) 419.

(27) H.P. Summers; Mon. Not. R. Astr. Soc. 169 (1974) 663.

(28) C.W. Allen; "Astrophysical Quantities (3rd Ed)" (University of London, 1973).

(29) H. Itoh; Publ. Astron. Soc. Japan 29 (1977) 813.

(30) S.M.R. Ansari, G. Elwert, and P. Mücklich; Z. Naturforsch. 25a (1970) 1781.

(31) C. Jordan; Mon. Not. R. Astr. Soc. 148 (1970) 17.

Table 1. Numerical Values of Parameters in Equations (2.12a, b)

Isosequence	H	He	Li	Be	B	C	N	O	F	Ne
$A_o(10^{-10}\ cm^{-3}s^{-1})$	10	16	3.0	1.0	13	0.88	5.6	4.2	3.3	1.6
ξ	2	2	1.45	1.5	2.1	2.3	1.7	1.7	1.65	2.65
W_o(eV)	9	9			3.3					2.2
K	1	2			2					1
ζ	2				1					2

Table 2. Element Abundances, log n_H = 12.00

Element	H	He	C	N	O	Ne	Mg	Si	S	Ca	Fe	Ni
(a)	12.0	11.3	8.7	7.8	8.5	7.6	7.5	7.7	7.3	6.3	7.7	6.7
(b)	12.00	10.93	8.52	7.96	8.82	7.92	7.42	7.52	7.20	6.30	7.60	6.30

Table 3. List of Calculations of Line Emission

Authors	Landini-Fossi (1970)	Mewe (1972b)	Tucker-Koren (1971)	Kato (1976)	Raymond-Smith (1977)	Stern et al. (1978)	Kato (1978)
Wavelength (Å)	1-100	1-220	1-70	1-250	1-200	100-1000	1-1000
Number of lines	40	320	453	795	512	657	934
Element abundances	(a)	(a)	(a)	(a)	(b)	(b)	(b)
Density effect	yes	yes	yes	yes	no	no	no
Ion abundances	(1)	Jordan	Jordan	Jordan	(2)	Jordan	Jordan

(1) Essentially the same as Jordan's.

(2) Different from Jordan's because of smaller ionization cross sections by Summers.

Table 4. Strong Ion Lines

Ion	W.L.(A)	f		log T_m [b]
MgXI	9.17	0.745		
	9.23		F [a]	6.8
	9.32		F	
NeIX	13.44	0.723		
	13.60		F	6.6
	13.70		F	
FeXVIII	13.40	0.250		
	14.30	1.700		6.9
FeXVII	15.00	2.2		6.7
	15.26	0.640		
	15.46	0.01		
	16.77	0.097		
	17.05		F	
OVIII	16.00	0.079		6.5
	19.00	0.416		
	21.60	0.694		
OVII	21.80		F	6.4
	22.09		F	
NVII	20.90	0.079		
	24.80	0.416		6.3
NVI	28.79	0.674		6.2
	29.08		F	
	29.50		F	
CVI	28.50	0.079		6.4
	33.70	0.416		
CV	40.27	0.647		6.1
	40.73		F	
	41.47		F	6.0
SiXI	48.14			
	49.22			6.3
SiX	49.70			6.2
	50.60	0.630		
	56.80	0.630		
SiIX	55.10	0.230		6.1
	55.30	0.630		

Table 4. Strong Ion Lines (Cont'd)

Ion	W.L.(A)	f	log T_m [b)]
SiVIII	50.00	0.310	6.0
SXII	36.00		6.4
	36.50	0.630	
SX	42.50	1.700	6.2
	47.00		
	52.00		
SIX	47.40	0.230	6.1
	49.20	0.800	
SVIII	46.00	0.250	6.0
	53.00	1.500	

a) Forbidden line

b) Temperature at which the ion abundance is maximum.

Figure Caption

Fig. 1. Ionization rate coefficients (a) for oxygen ions and (b) for iron ions. The solid and dashed curves show the rate by auto-ionization and by direct ionization, respectively. Recombination rate coefficients (c) for oxygen ions and (d) for iron ions. The solid curves in (c) represent α_d by Aldrovandi and Péquinot (1973),[12] and the solid and dot-dashed curves in (d) indicate $(\alpha_r + \alpha_d)$ by Jocobs et al (1977)[15],[16] and α_d by Ansari et al (1970),[30] respectively. The dashed curves show the radiative recombination coefficients α_r.

Fig. 2. The time dependent ion abundances of oxygen ions. (a) Ionizing plasma for a constant temperature KT = 300 eV and n(OVII)/n(O) = 1.0 for the initial ion abundances. The solid curves represent the results including dielectronic recombination and autoionization, whereas the dashed curves are those neglecting these two processes. (b) Recombining plasma for a constant temperature KT = 100 eV and n(OIX)/n(O) = 1.0 for the initial abundances.

Fig. 3. The ionization e uilibrium for Fe ions calculated by Jacobs et al (1977)[15],[16] (solid lines). The dashed lines due to Jordan (1969)[10] are shown for comparison.

Fig. 4. Intensities per ion and per electron of strong lines as a function of temperature under ionization equilibrium. The numbers in the parantheses represent the energies of lines in eV, and the energy range of the lines is indicated in the upper right corner. (a) O ions in the range 500 - 1000 eV, (b) O ions in 60 - 100 eV, (c) S ions, (d) Fe ions 500 - 1000 eV, (e) Fe ions in 100 - 500 eV, and (f) Fe ions in 60 - 100 eV.

Fig. 5. Radiation loss rate per electron and per atom of atomic number Z for H, He, C, N, O, Ne, Mg, Si, S, Ca, Fe and Ni ions.

Fig. 6. Contribution of strong lines to the total line emission. The numbers indicate the wavelengths of the lines in Å. (a) O ions, (b) S ions, and (c) Fe ions. The dashed line in (c) shows the total emission rate obtained with the ion abundances by Jordan (1969,[10] 1970[31]), whereas the solid lines by Jacobs et al (1977).[15],[16]

Fig. 7. The ion abundances in equilibrium state for solar corona (solid curves) and for a thin plasma without density effect (dashed curves), after Jordan (1969).[10] (a) O ions, (b) Fe ions.

Fig. 8. Comparison of equilibrium abundances of Mg ions calculated by Jordan (1969)[10] (solid lines) and by Summers (1974)[27] (dashed lines). The difference is caused by that of the ionization rate coefficient.

Fig. 9. Comparison of calculated spectra at log T = 6.2 (T_e = 137 eV) by Landini and Fossi (1970),[24] by Tucker and Koren (1971)[23] and by Kato (1976).[1]

Fig.10. The line intensities of iron ions calculated by Kato[1] (1976) (solid curves), by Stern et al (1976)[25] (dashed curves), by Raymond and Smith (1977)[26] (dott-dashed curves), and by Mewe (1972,[21] 1975[22]) (dotted curves) are compared as functions of temperature. The numbers represent the wavelengths of the lines in Å.

Fig.11. The emission powers of strong lines of typical elements for a thin plasma of cosmic abundances (solid curved). The power of continuum in the wavelength range 1 Å at the wavelength indicated in the paranthesis (dashed curved) are also shown for the sake of comparison.

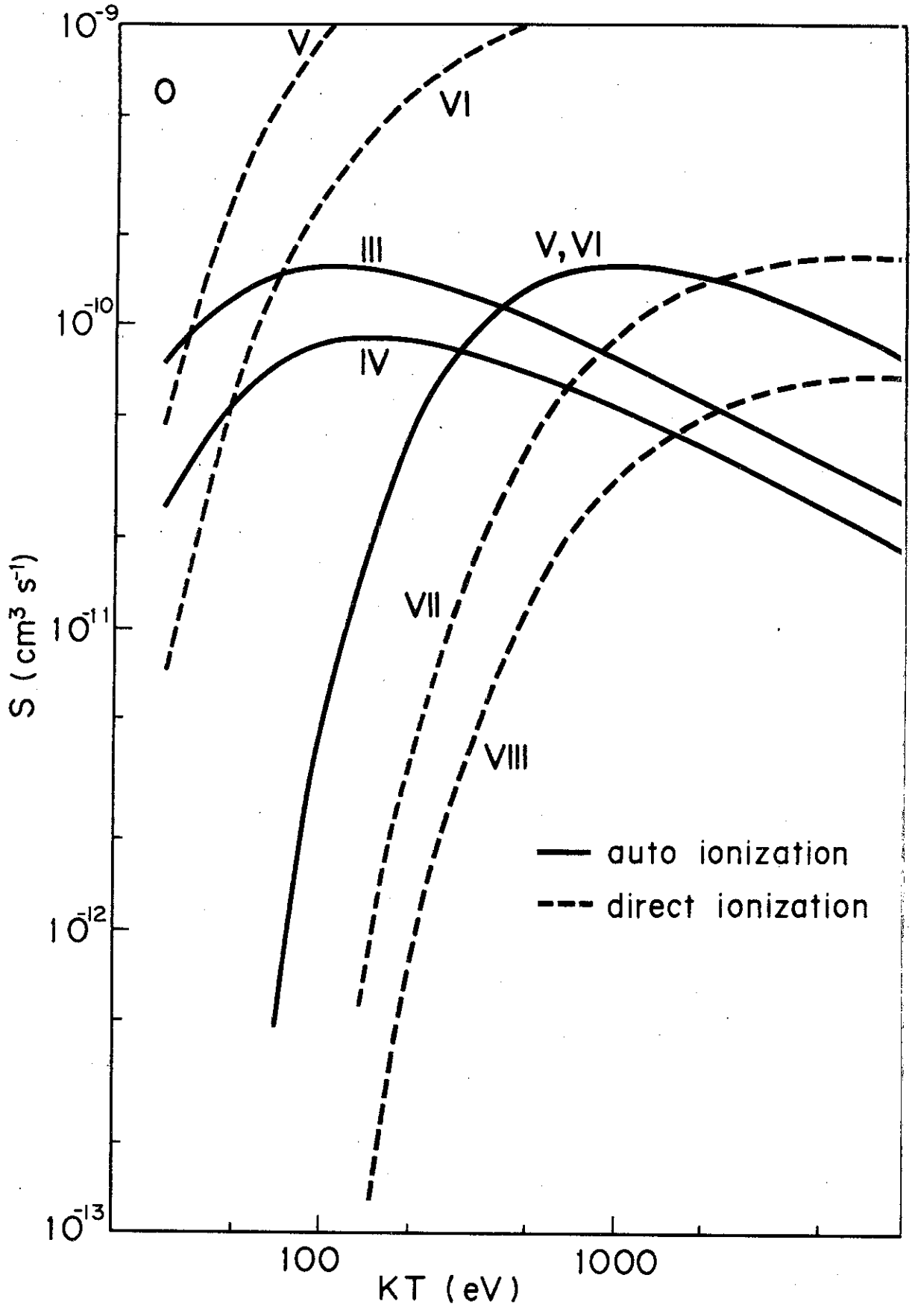
10^-9
10^-10
10^-11
10^-12
10^-13
S (cm^3 s^-1)
O
V
VI
III
V, VI
IV
VII
VIII
auto ionization
direct ionization
100
1000
KT (eV)

Fig. 1(a)

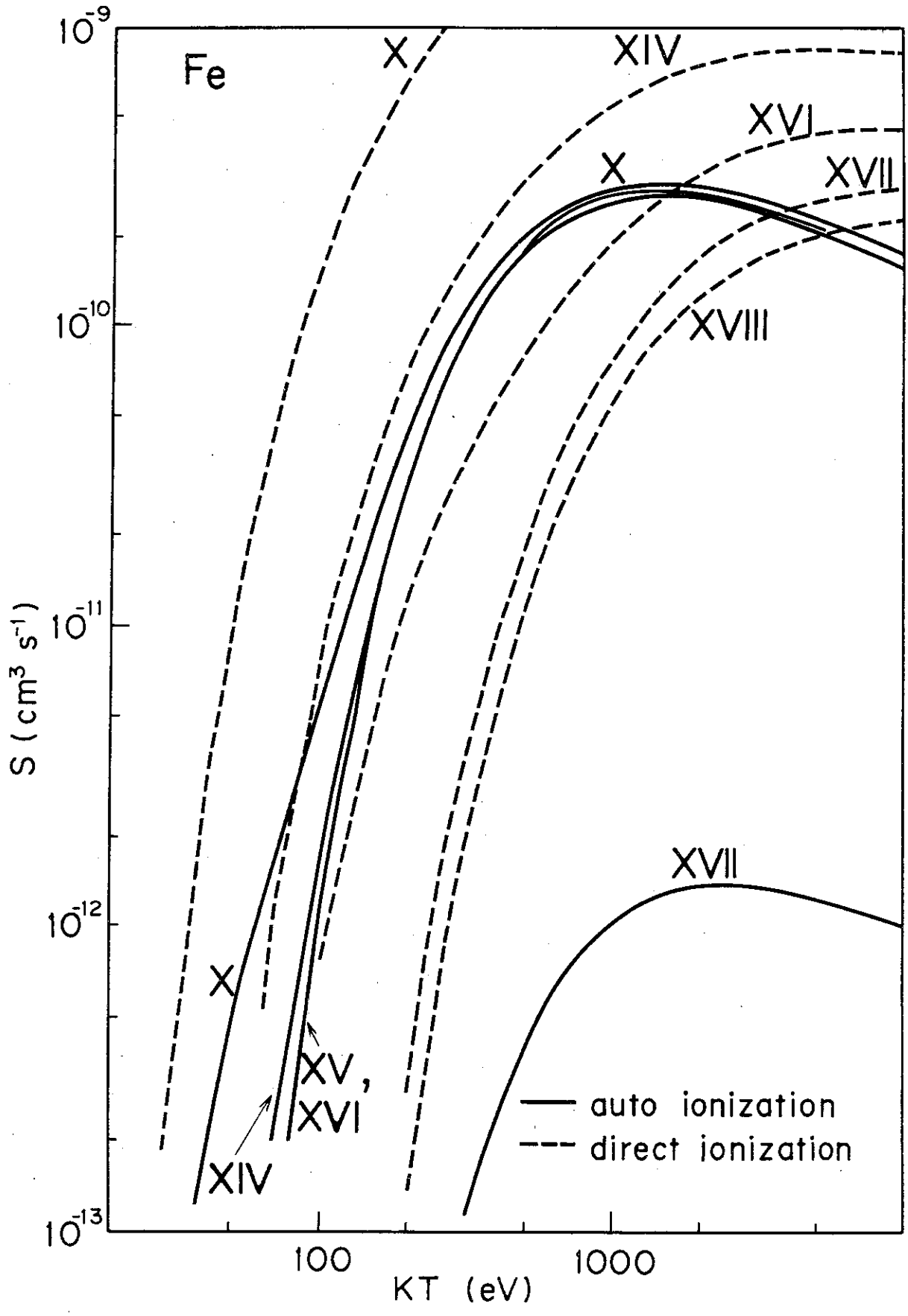
Fe
X
XIV
XVI
X
XVII
XVIII
X
XV,
XVI
XIV
XVII
auto ionization
direct ionization
S (cm³ s⁻¹)
KT (eV)
10⁻⁹
10⁻¹⁰
10⁻¹¹
10⁻¹²
10⁻¹³
100
1000

Fig. 1(b)

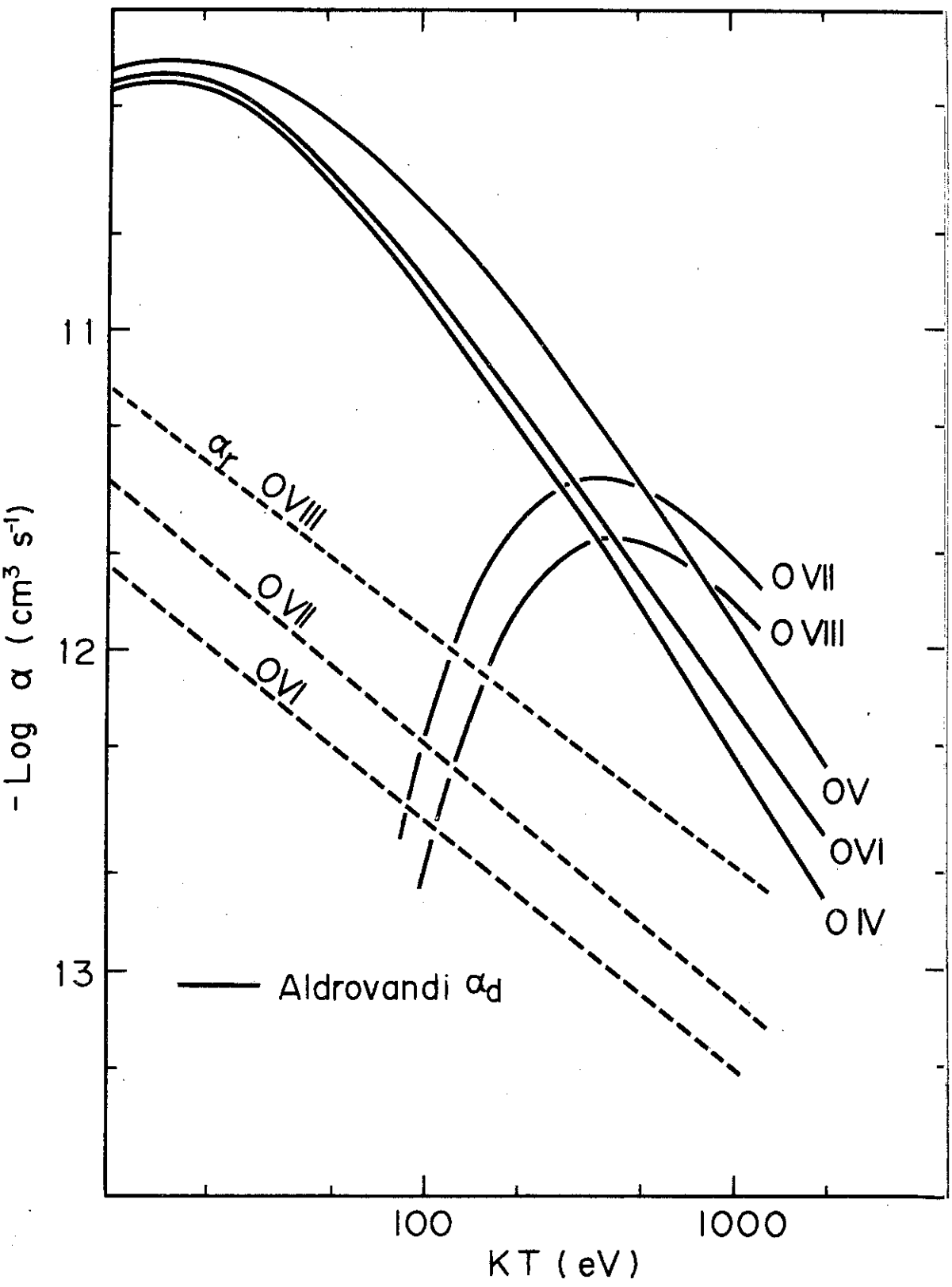
11
12
13
- Log α (cm³ s⁻¹)
αr OVIII
OVII
OVI
O VII
O VIII
OV
OVI
O IV
Aldrovandi αd
100
1000
KT (eV)

Fig. 1(c)

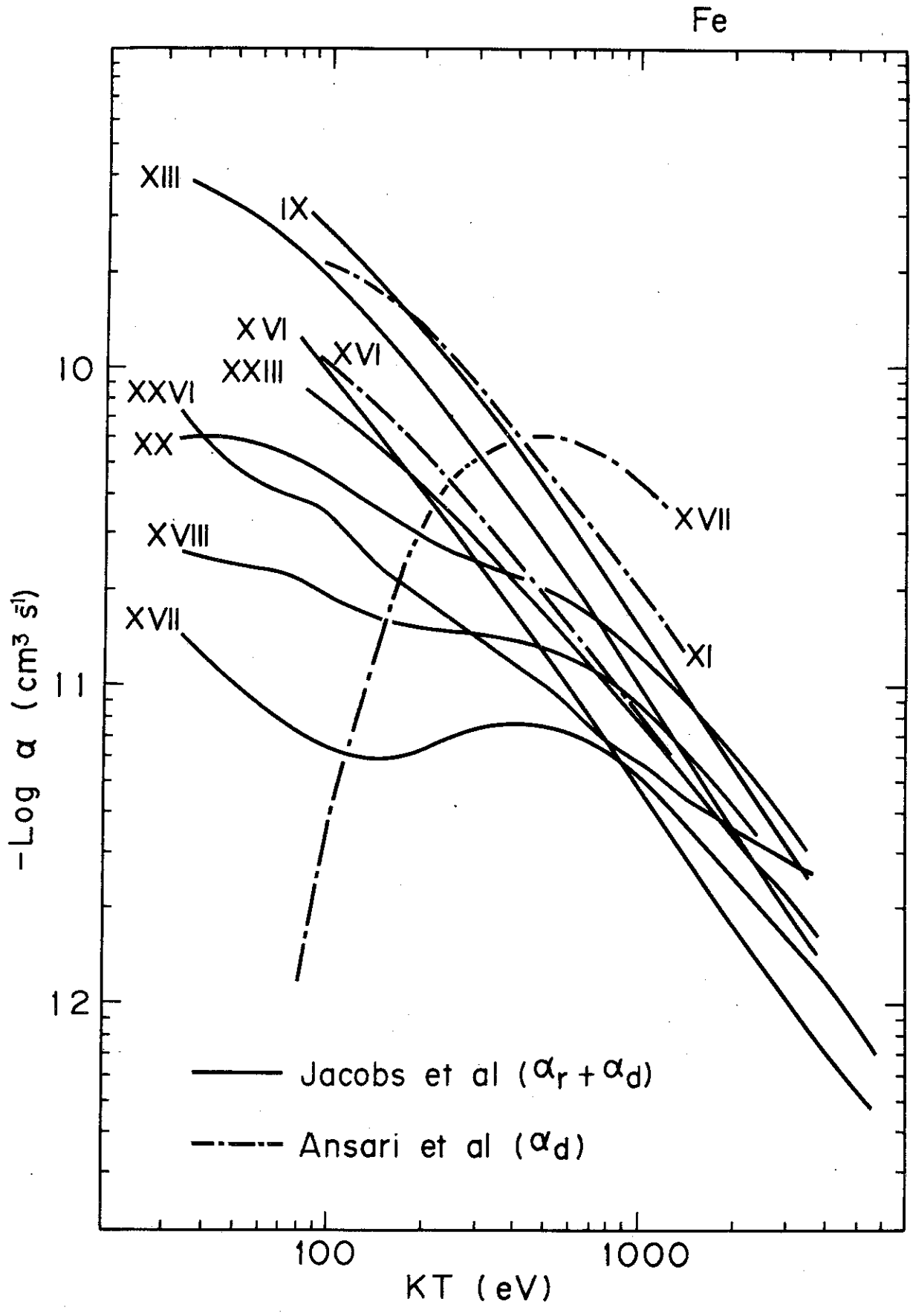
Fe
XIII
IX
XVI
XVI
XXIII
XXVI
XX
XVIII
XVII
XVII
XI
10
11
12
-Log α (cm³ s⁻¹)
Jacobs et al (αr + αd)
Ansari et al (αd)
100
1000
KT (eV)

Fig. 1(d)

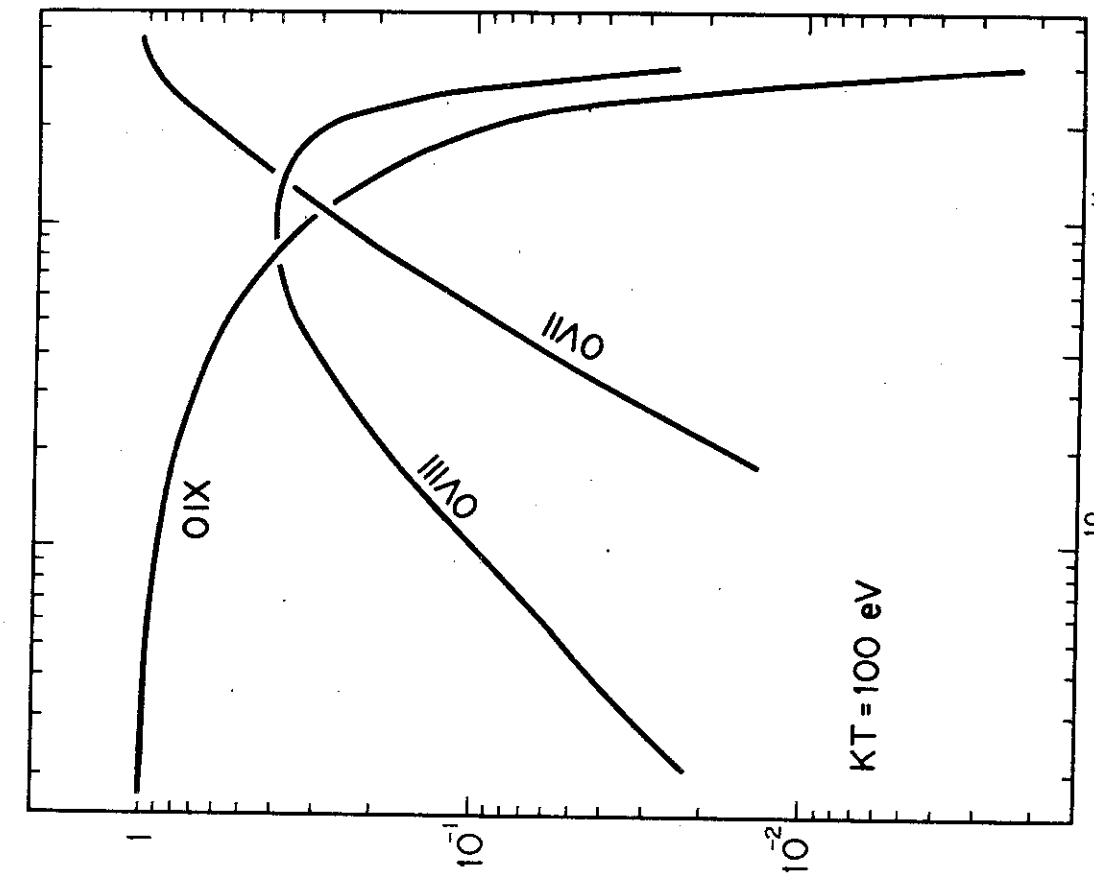
OIX
OVIII
OVIII
KT=100 eV
1
10^{-1}
10^{-2}
10^{10}
10^{11}
nt (cm^{-3}s)

Fig. 2 (b)

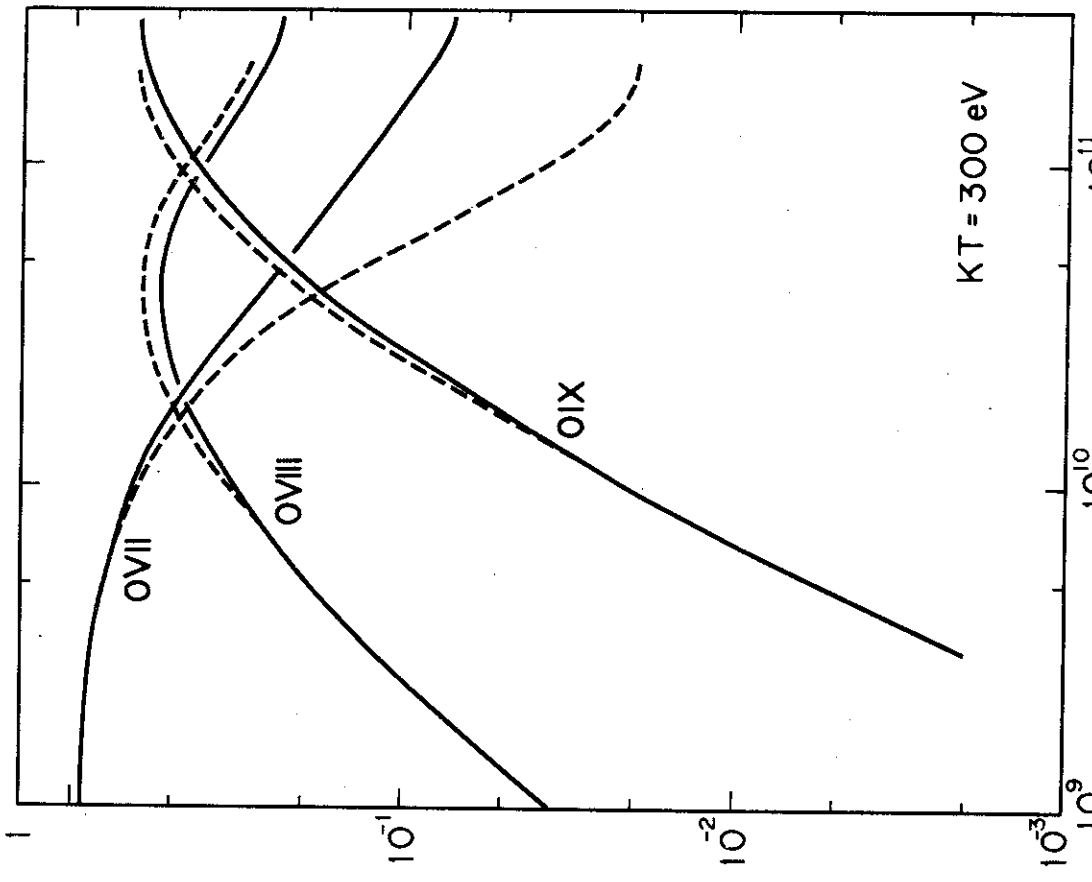
OVII
OVIII
OIX
KT=300 eV
1
10^{-1}
10^{-2}
10^{-3}
10^{9}
10^{10}
10^{11}
nt (cm^{-3}s)

Fig. 2 (a)

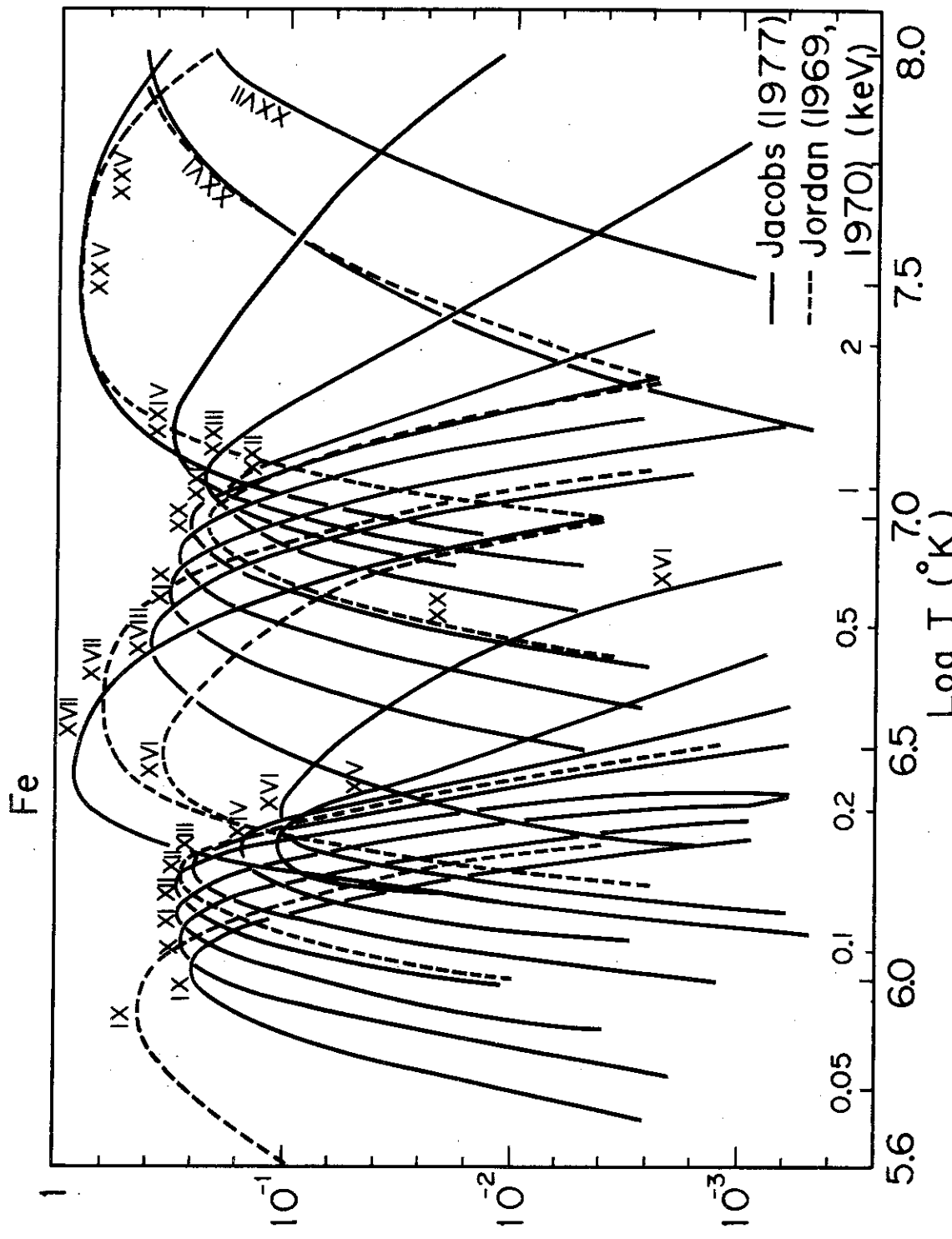
Fe
Jacobs (1977)
Jordan (1969, 1970) (keV)
Log T (°K)
5.6
6.0
6.5
7.0
7.5
8.0
0.05
0.1
0.2
0.5
1
2
1
10^{-1}
10^{-2}
10^{-3}

Fig. 3

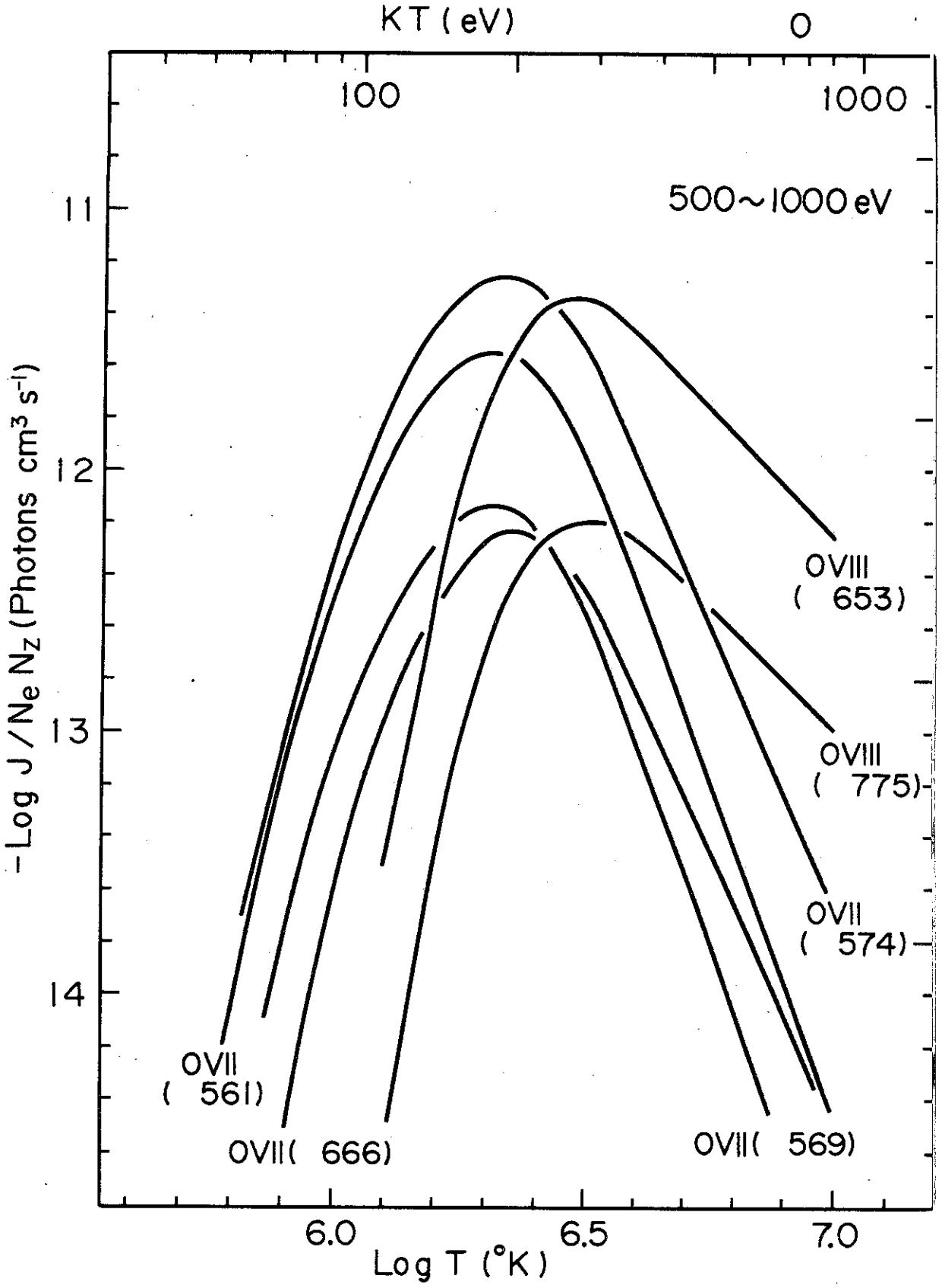
KT (eV)
0
100
1000
500~1000 eV
11
12
13
14
-Log J/Ne Nz (Photons cm3 s-1)
OVIII
(653)
OVIII
(775)
OVII
(574)
OVII
(561)
OVII(666)
OVII(569)
6.0
6.5
7.0
Log T (°K)

Fig. 4(a)

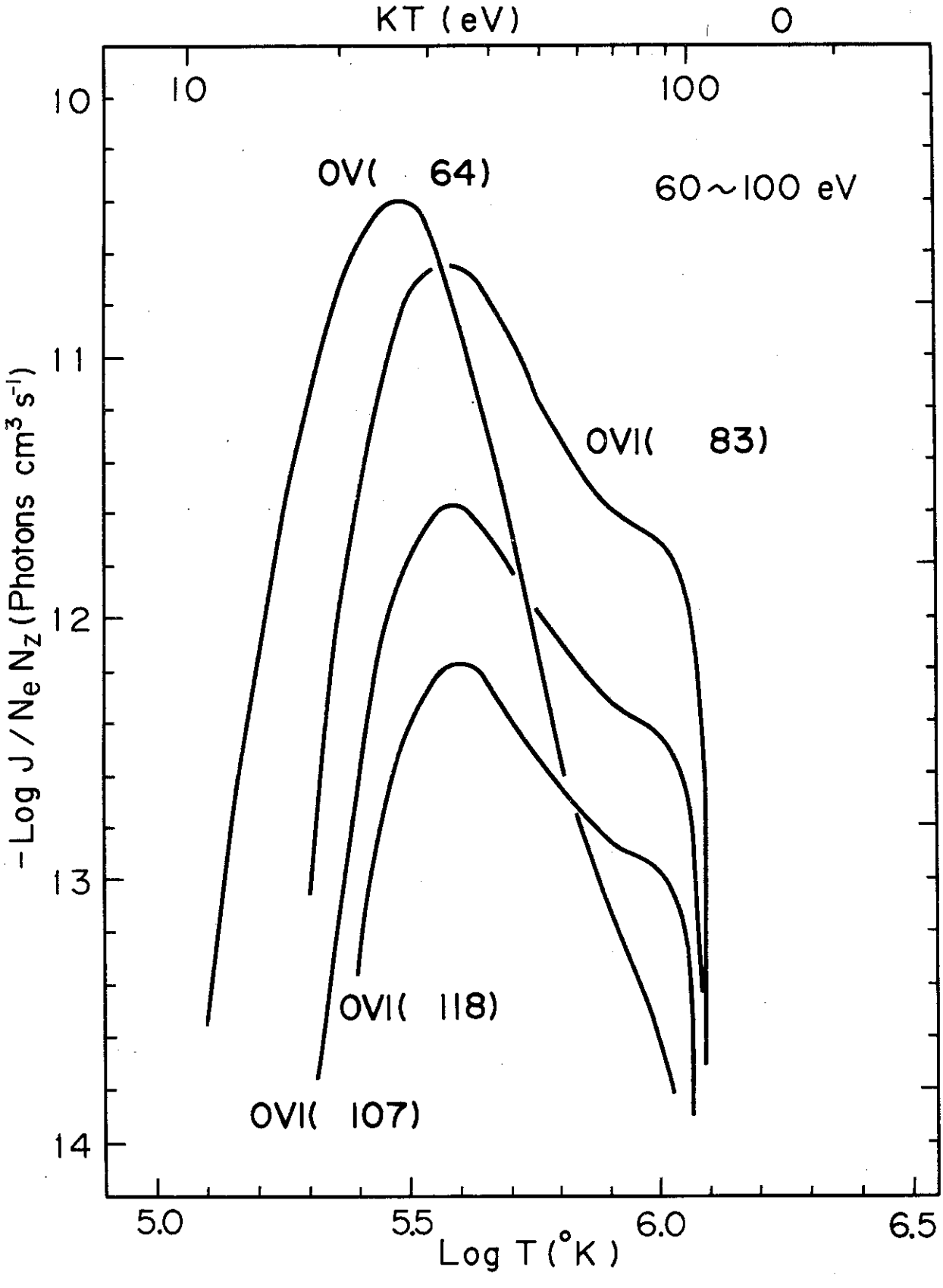
KT (eV)
10
100
0
OV(64)
60~100 eV
OVI(83)
OVI(118)
OVI(107)
10
11
12
13
14
-Log J / Ne Nz (Photons cm3 s-1)
5.0
5.5
6.0
6.5
Log T (°K)

Fig. 4 (b)

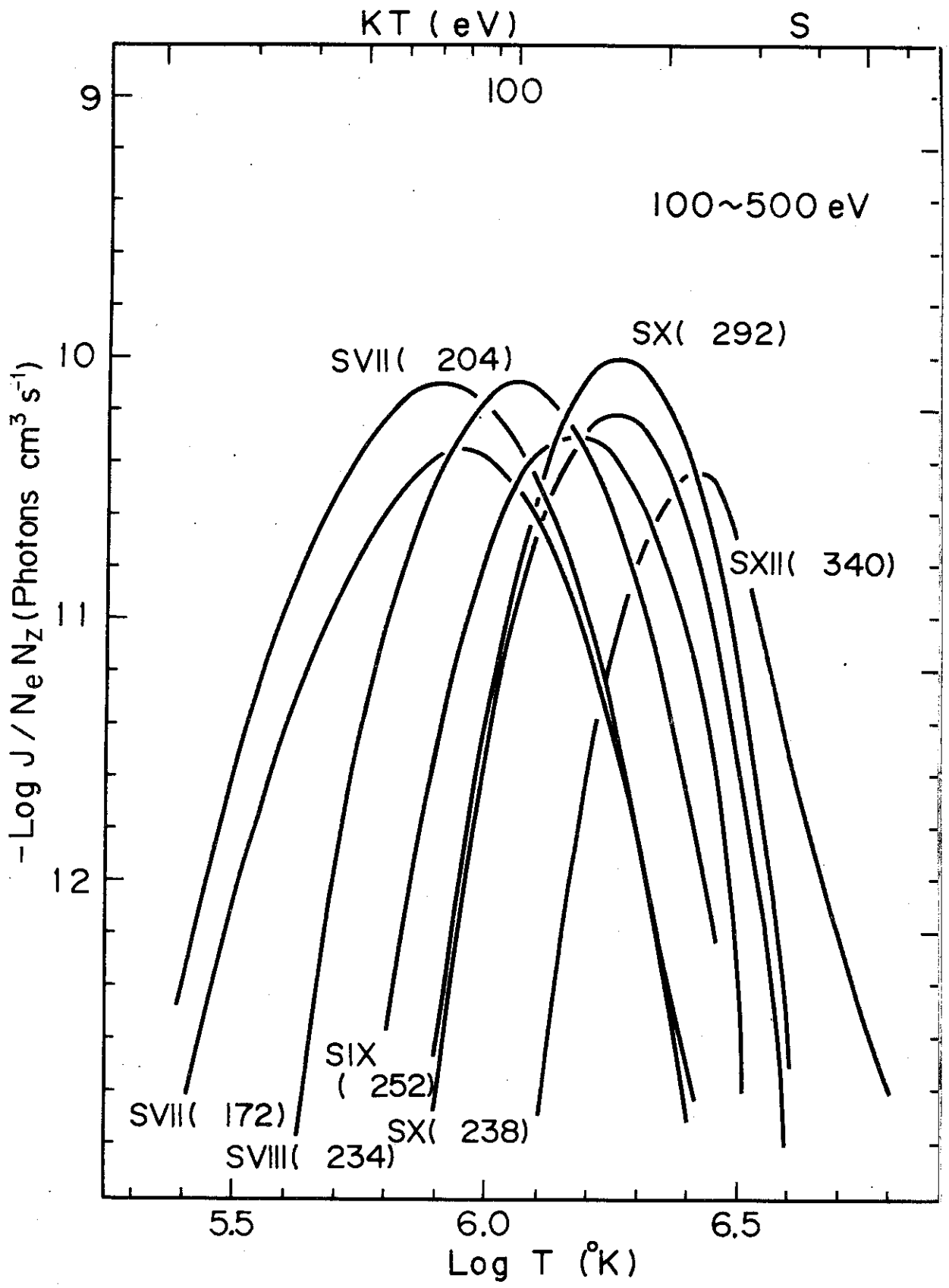
KT (eV)
S
100
9
10
11
12
100~500 eV
SX(292)
SVII(204)
SXII(340)
SIX
(252)
SVII(172)
SVIII(234)
SX(238)
-Log J / Ne Nz (Photons cm3 s-1)
5.5
6.0
6.5
Log T (°K)

Fig. 4 (c)

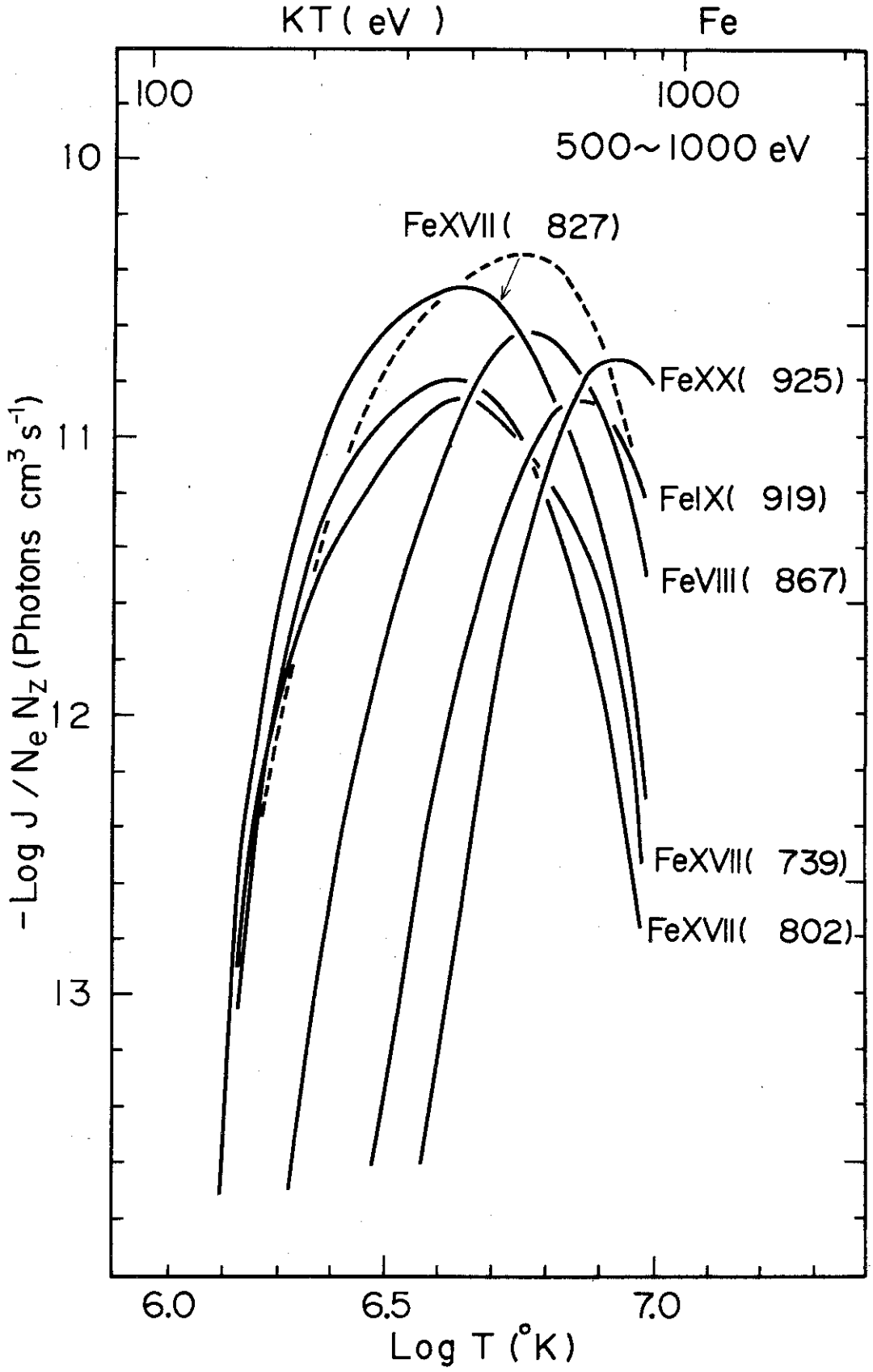
KT (eV)
Fe
100
1000
500~1000 eV
10
11
12
13
FeXVII(827)
FeXX(925)
FeIX(919)
FeVIII(867)
FeXVII(739)
FeXVII(802)
-Log J / Ne Nz (Photons cm3 s-1)
6.0
6.5
7.0
Log T (°K)

Fig. 4(d)

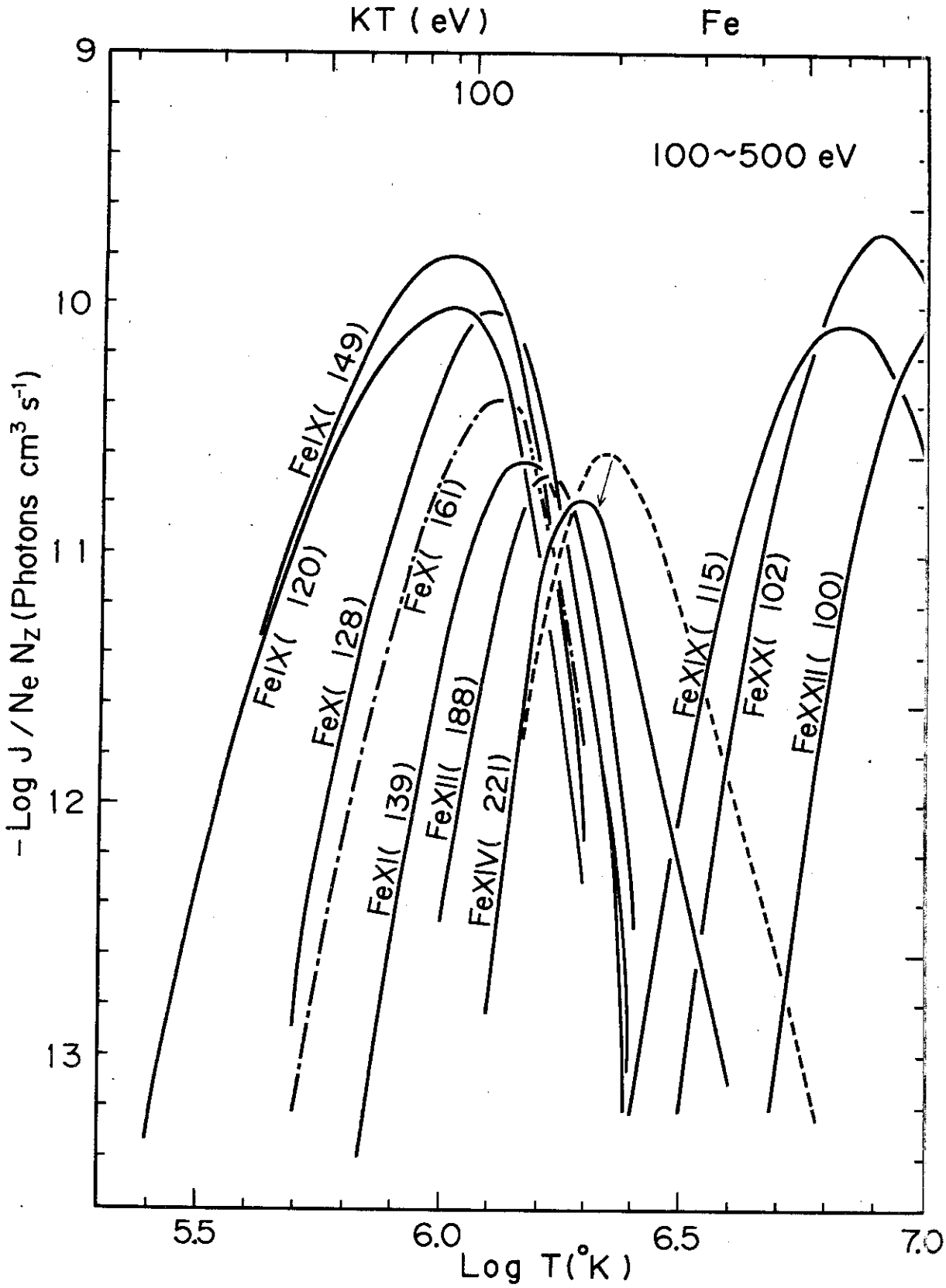
KT (eV)
Fe
9
100
100~500 eV
10
11
12
13
-Log J / Ne Nz (Photons cm3 s-1)
FeIX(149)
FeIX(120)
FeX(128)
FeX(161)
FeXI(139)
FeXII(188)
FeXIV(221)
FeXIX(115)
FeXX(102)
FeXXII(100)
5.5
6.0
6.5
7.0
Log T(°K)

Fig. 4(e)

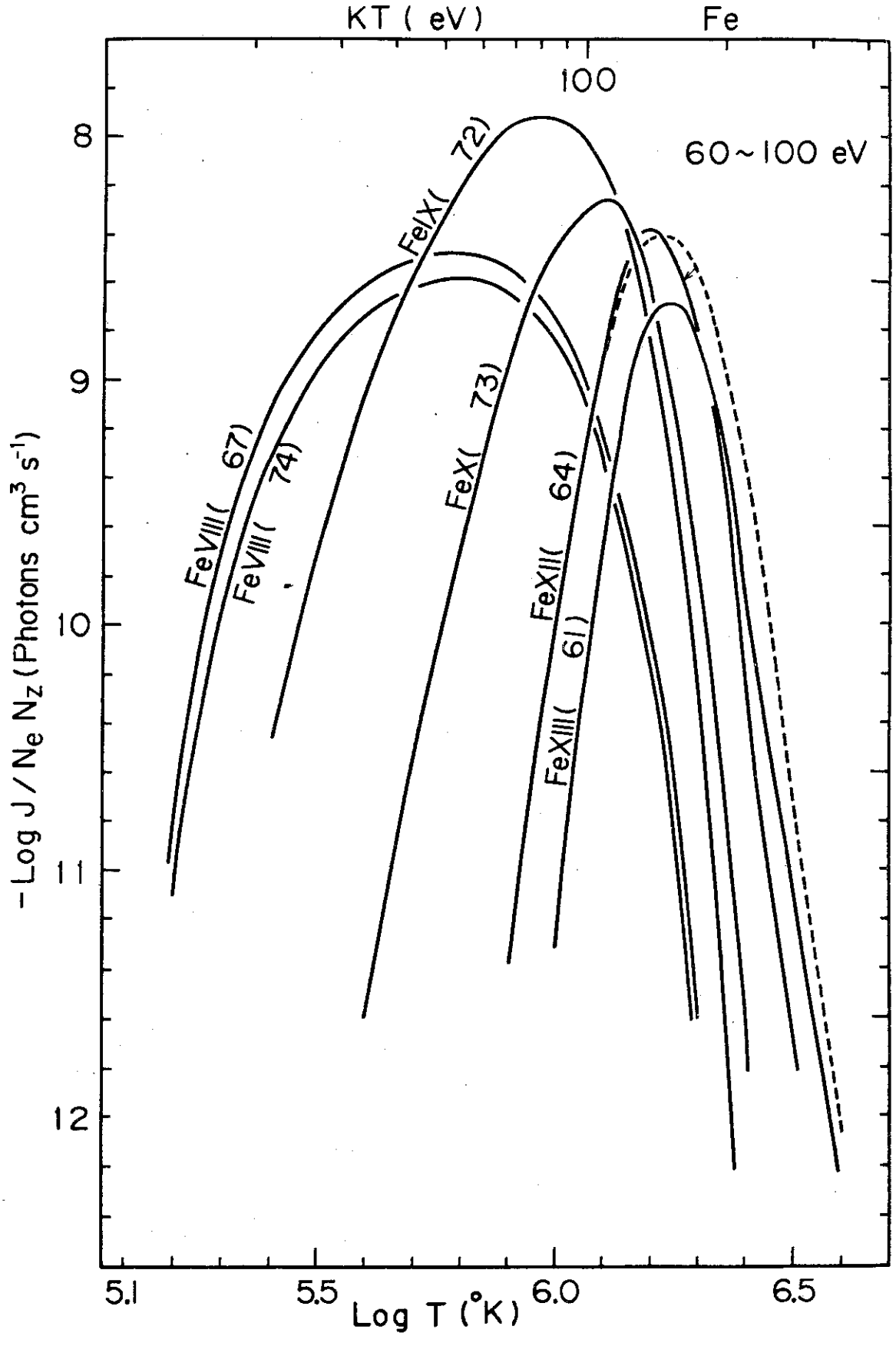
KT (eV)
Fe
100
60~100 eV
FeIX(72)
FeVIII(67)
FeVIII(74)
FeX(73)
FeXIII(64)
FeXIII(61)
-Log J / Ne Nz (Photons cm3 s-1)
8
9
10
11
12
5.1
5.5
6.0
6.5
Log T (°K)

Fig. 4 (f)

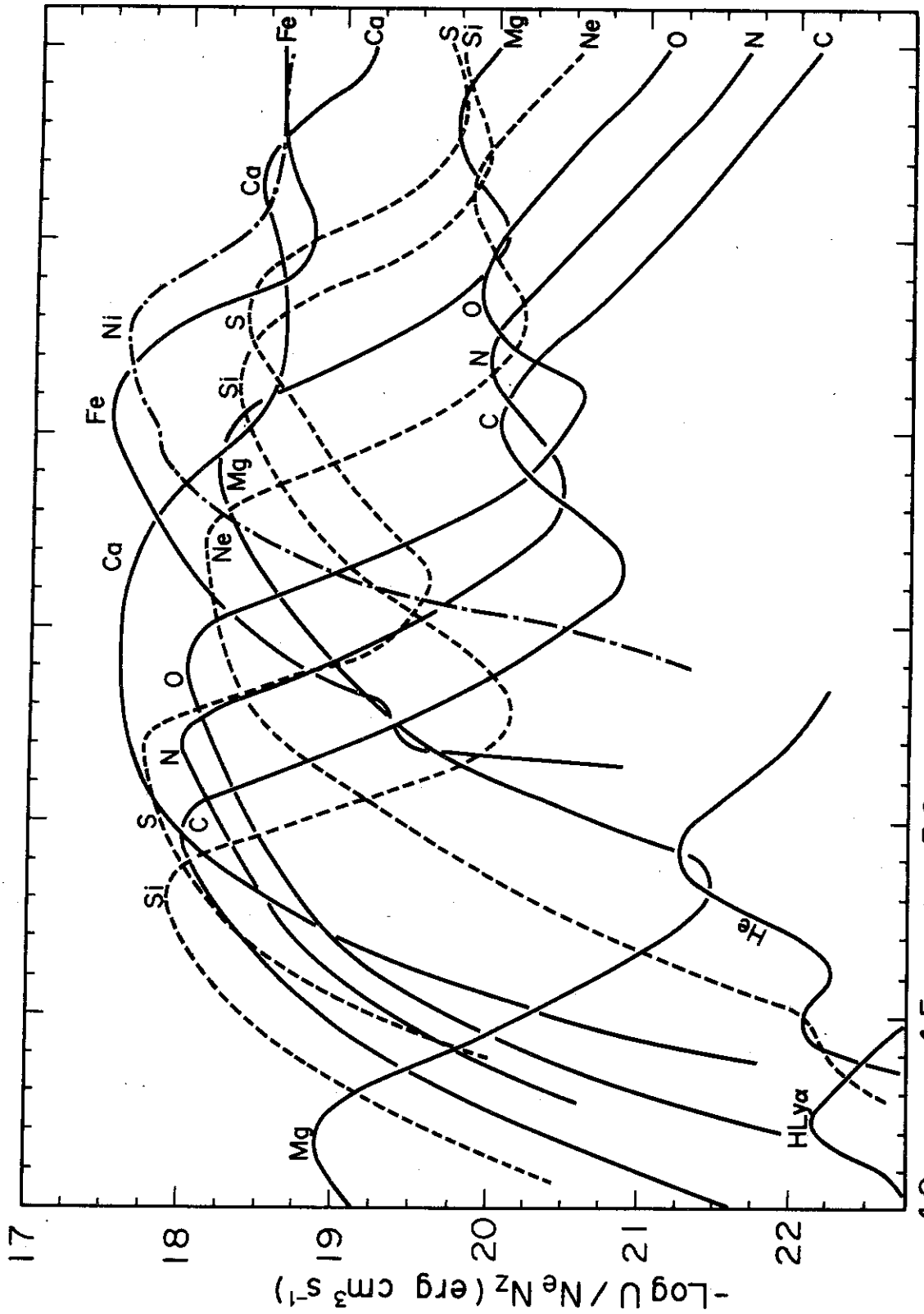
-Log U / Ne Nz (erg cm3 s-1)
17
18
19
20
21
22
Log T (°K)
4.0
4.5
5.0
5.5
6.0
6.5
7.0
Fe
Ca
S
Si
Mg
Ne
O
N
C
Ni
He
HLyα

Fig. 5

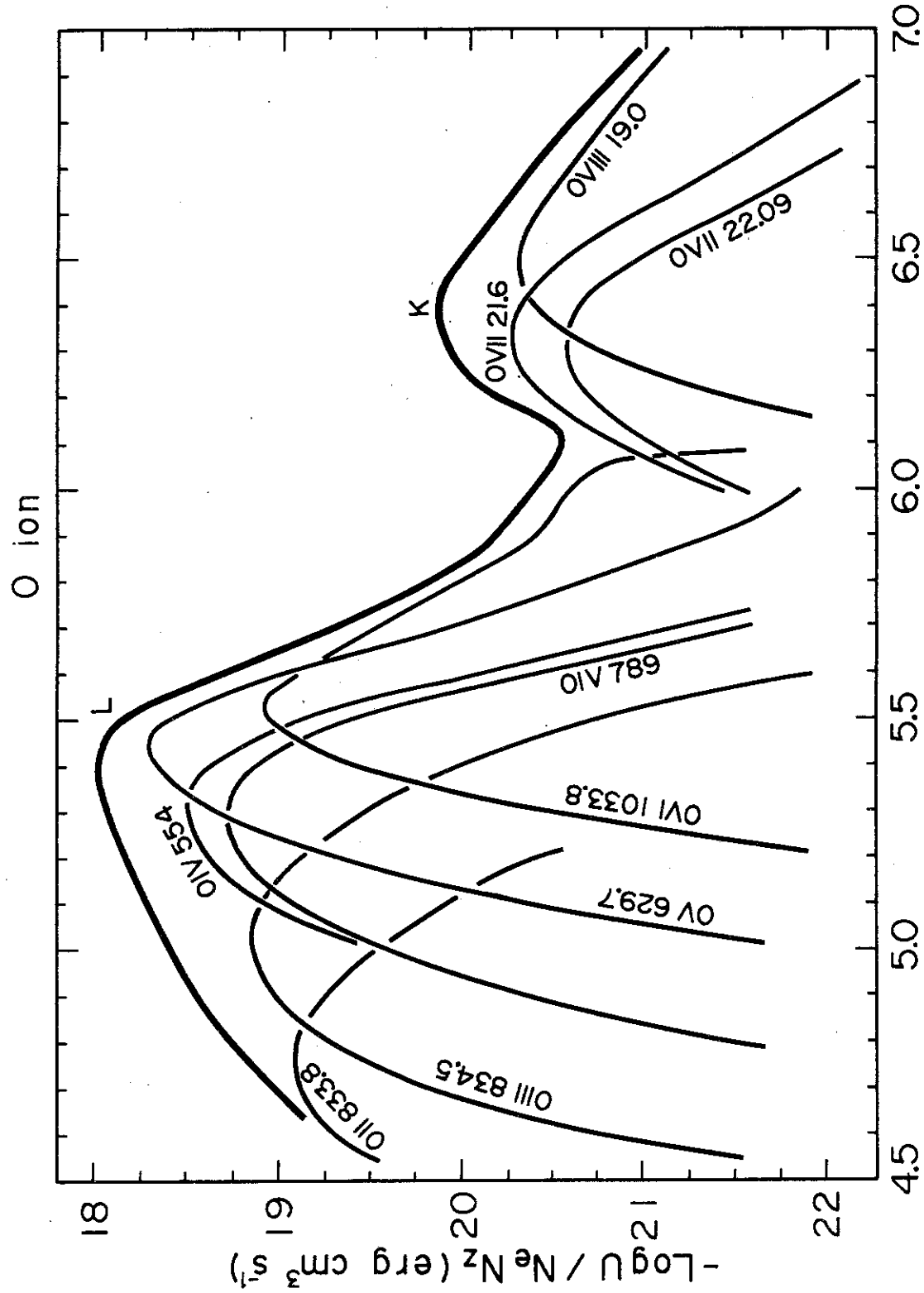
O ion
K
L
OVIII 19.0
OVII 22.09
OVII 21.6
OIV 789
OVI 1033.8
OV 629.7
OIV 554
OIII 834.5
OII 833.8
-Log U / Ne Nz (erg cm3 s-1)
Log T (°K)
18
19
20
21
22
4.5
5.0
5.5
6.0
6.5
7.0

Fig. 6(a)

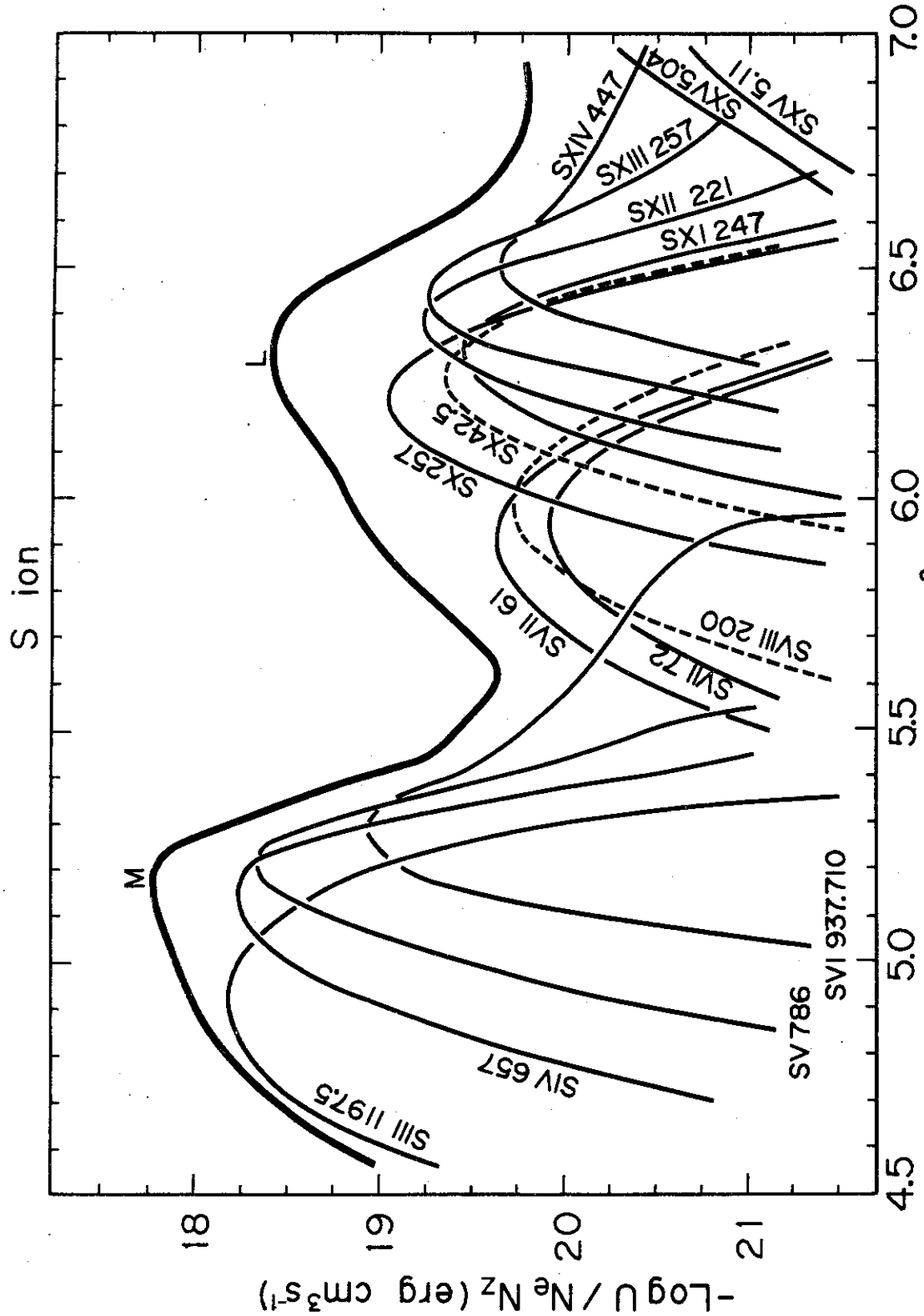
S ion
SXIV 447
SXV 5.04
SXV 5.11
SXIII 257
SXII 221
SXI 247
SX 425
SX 257
SVII 61
SVIII 200
SVII 72
SIV 657
SV 786
SVI 937.710
SIII 1197.5
L
M
-Log U / Ne Nz (erg cm3s-1)
Log T (°K)
18
19
20
21
4.5
5.0
5.5
6.0
6.5
7.0

Fig. 6 (b)

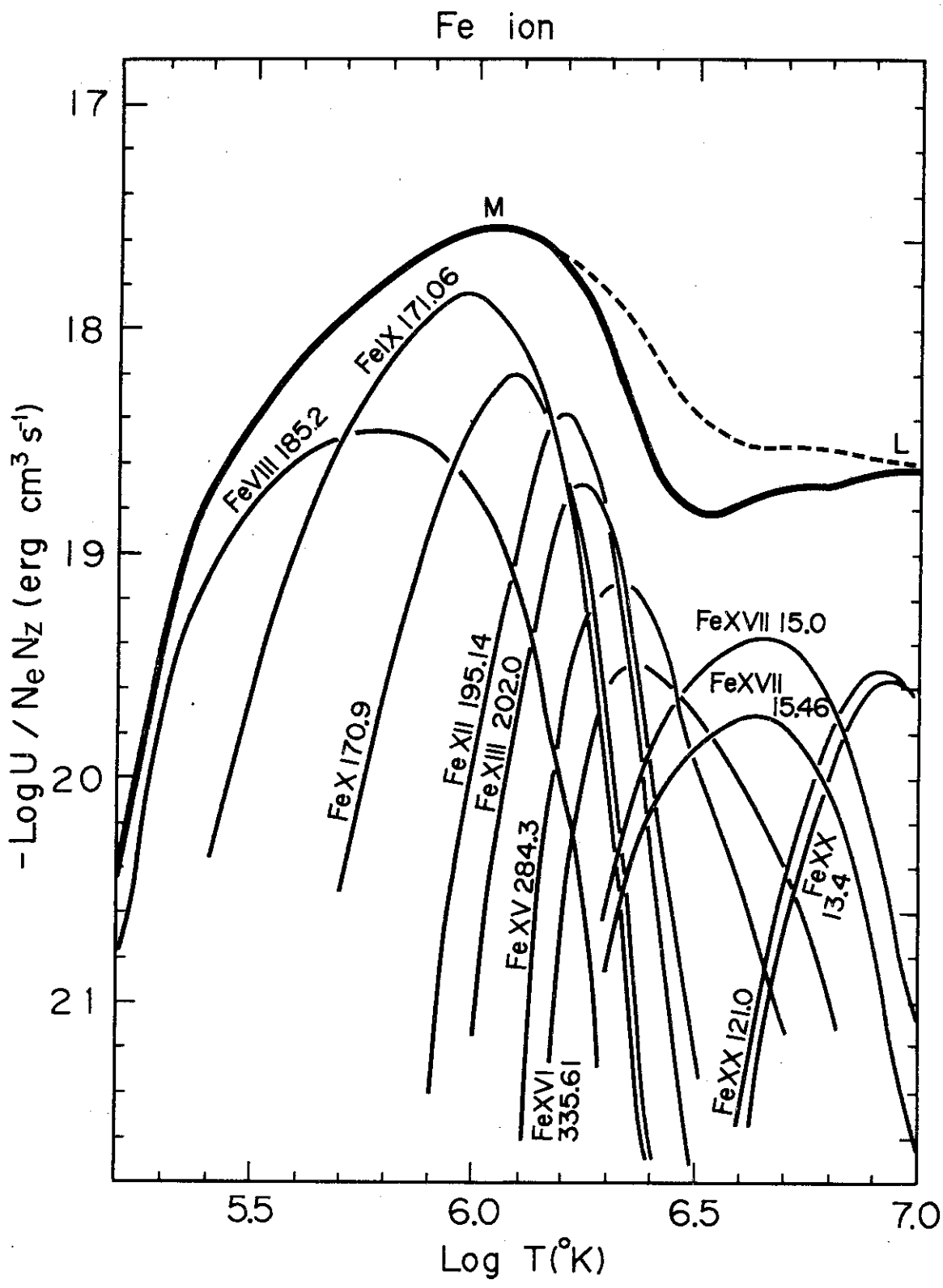
Fe ion
17
18
19
20
21
M
L
FeVIII 185.2
FeIX 171.06
FeX 170.9
FeXII 195.14
FeXIII 202.0
FeXV 284.3
FeXVI 335.61
FeXVII 15.0
FeXVII 15.46
FeXX 121.0
FeXX 13.4
-Log U / Ne Nz (erg cm3 s-1)
5.5
6.0
6.5
7.0
Log T(°K)

Fig. 6(c)

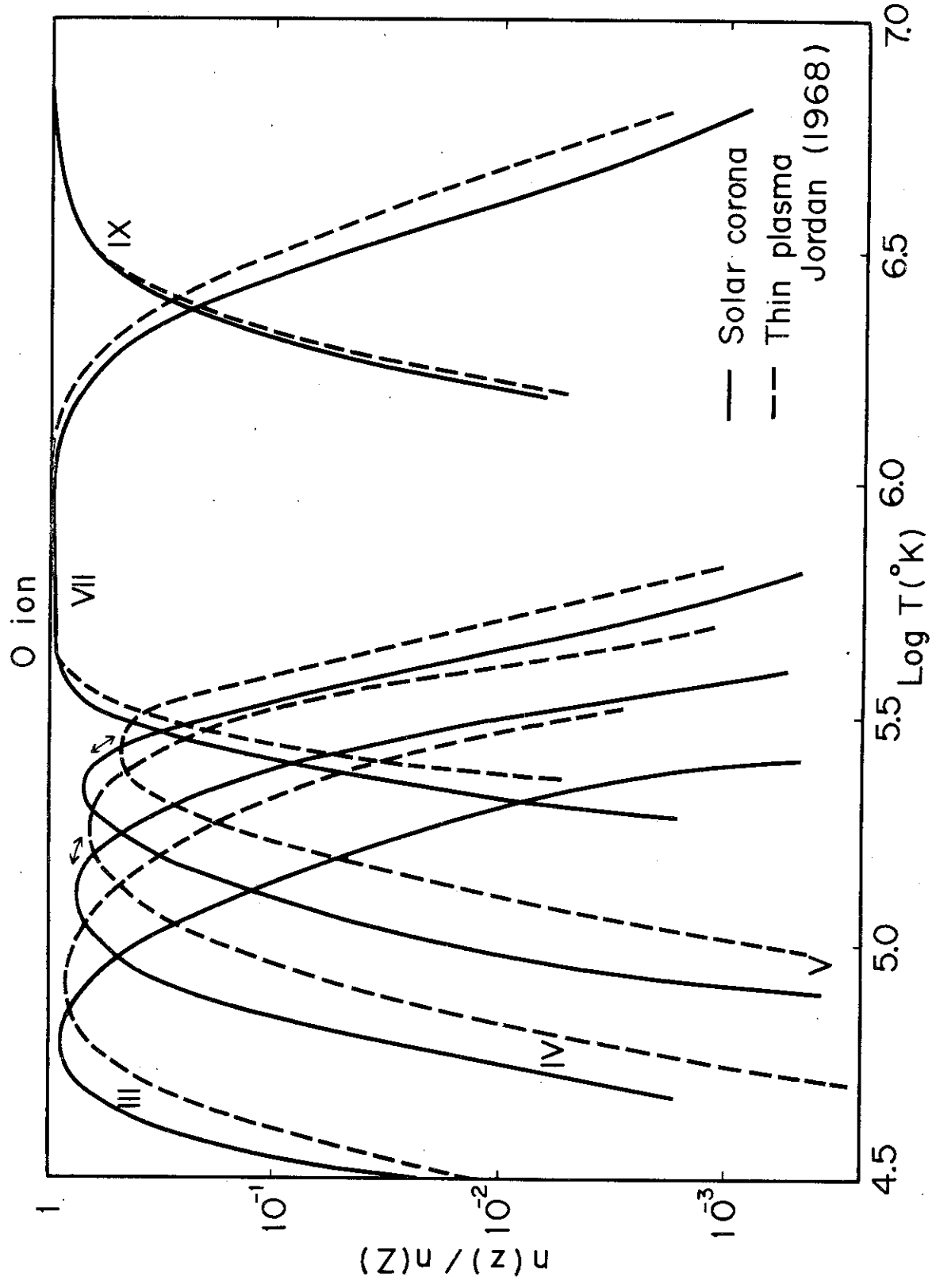
O ion
VII
IX
III
IV
V
Solar corona
Thin plasma
Jordan (1968)
n(z) / n(Z)
1
10^{-1}
10^{-2}
10^{-3}
4.5
5.0
5.5
6.0
6.5
7.0
Log T(°K)

Fig. 7(a)

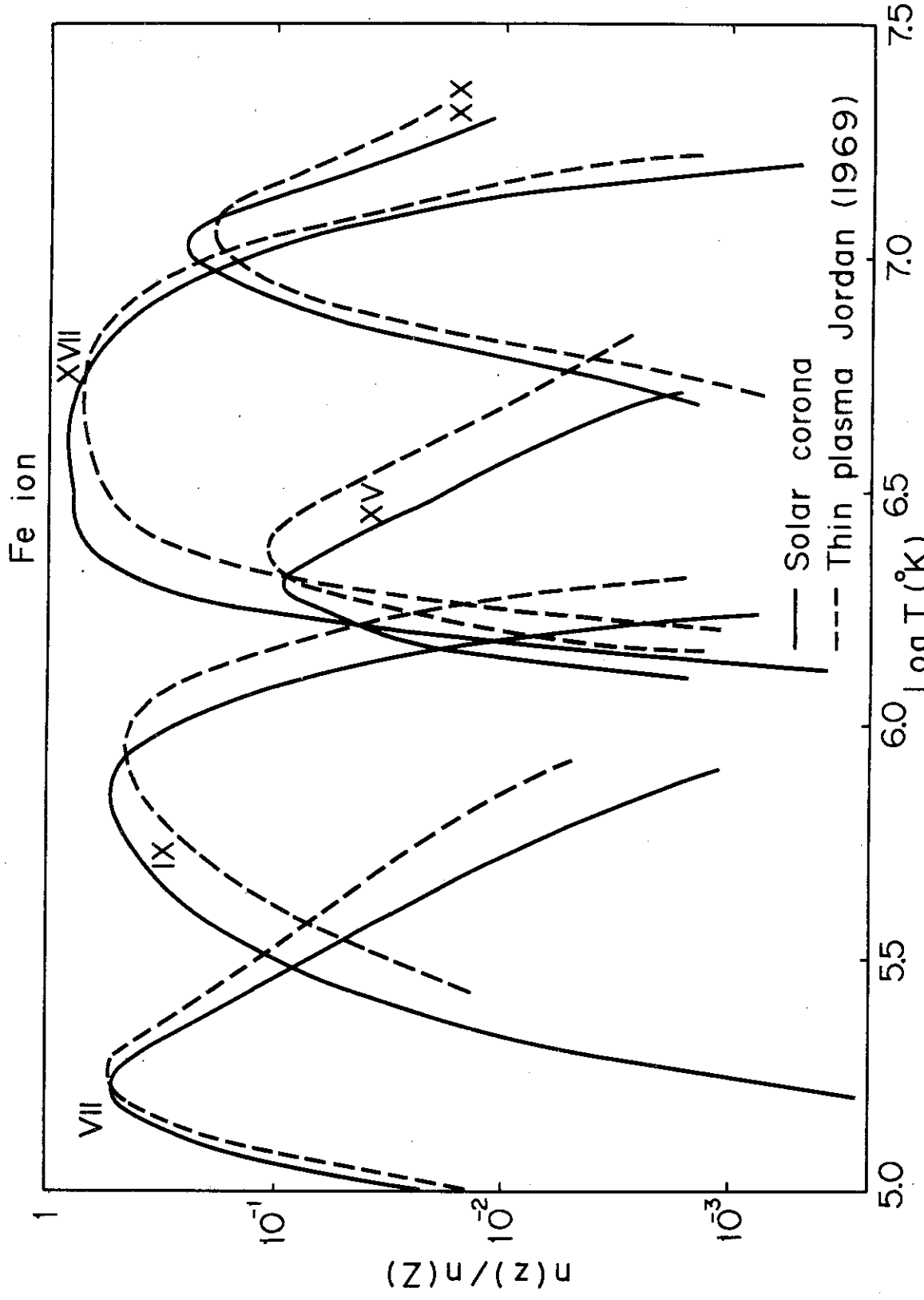
Fe ion
VII
IX
XV
XVII
XX
Solar corona
Thin plasma Jordan (1969)
n(z)/n(Z)
1
10^-1
10^-2
10^-3
5.0
5.5
6.0
6.5
7.0
7.5
Log T (°K)

Fig. 7 (b)

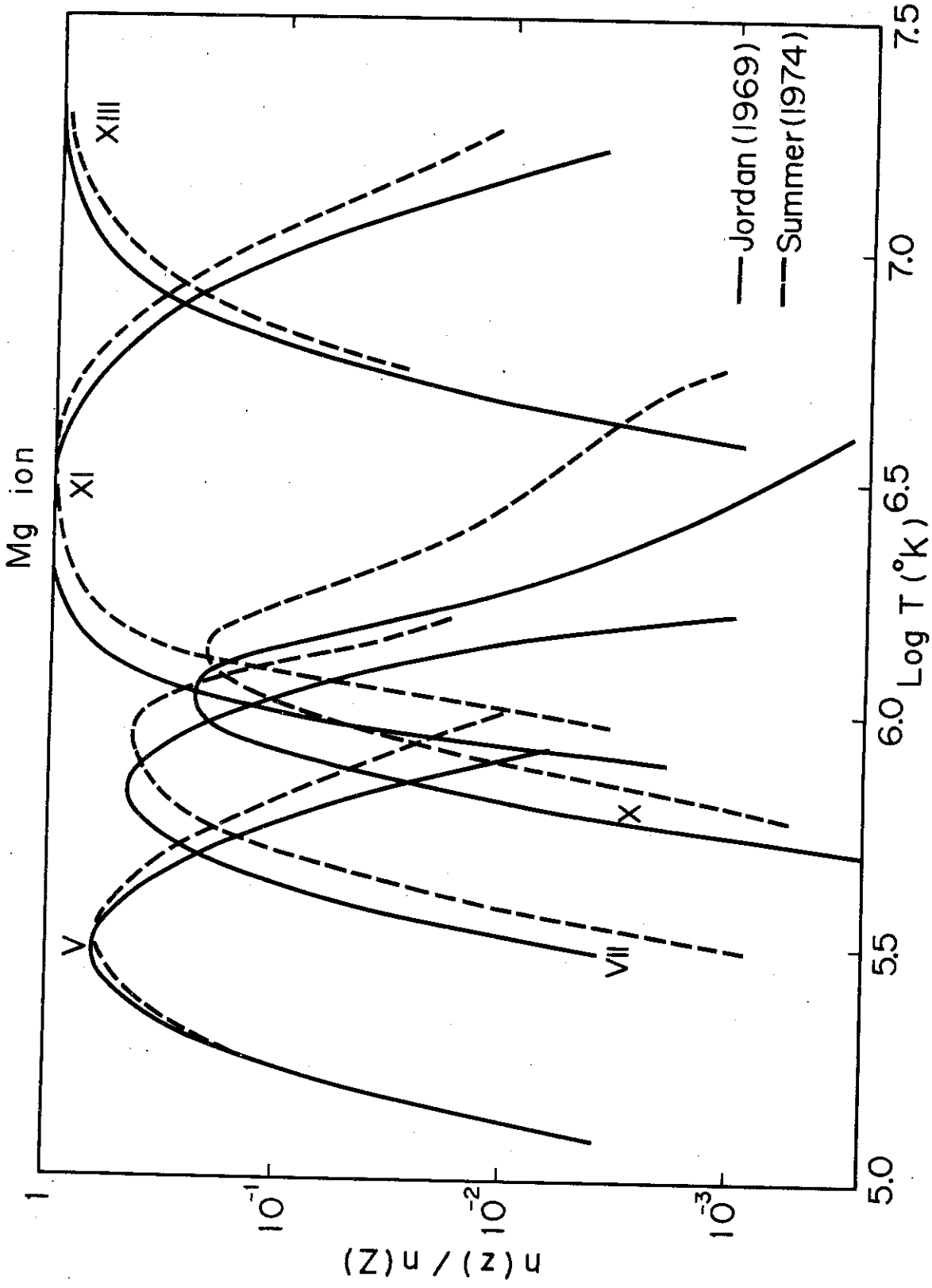
Mg ion
XIII
XI
V
X
VII
Jordan (1969)
Summer (1974)
n (z) / n (Z)
1
10^{-1}
10^{-2}
10^{-3}
5.0
5.5
6.0
6.5
7.0
7.5
Log T (°K)

Fig. 8

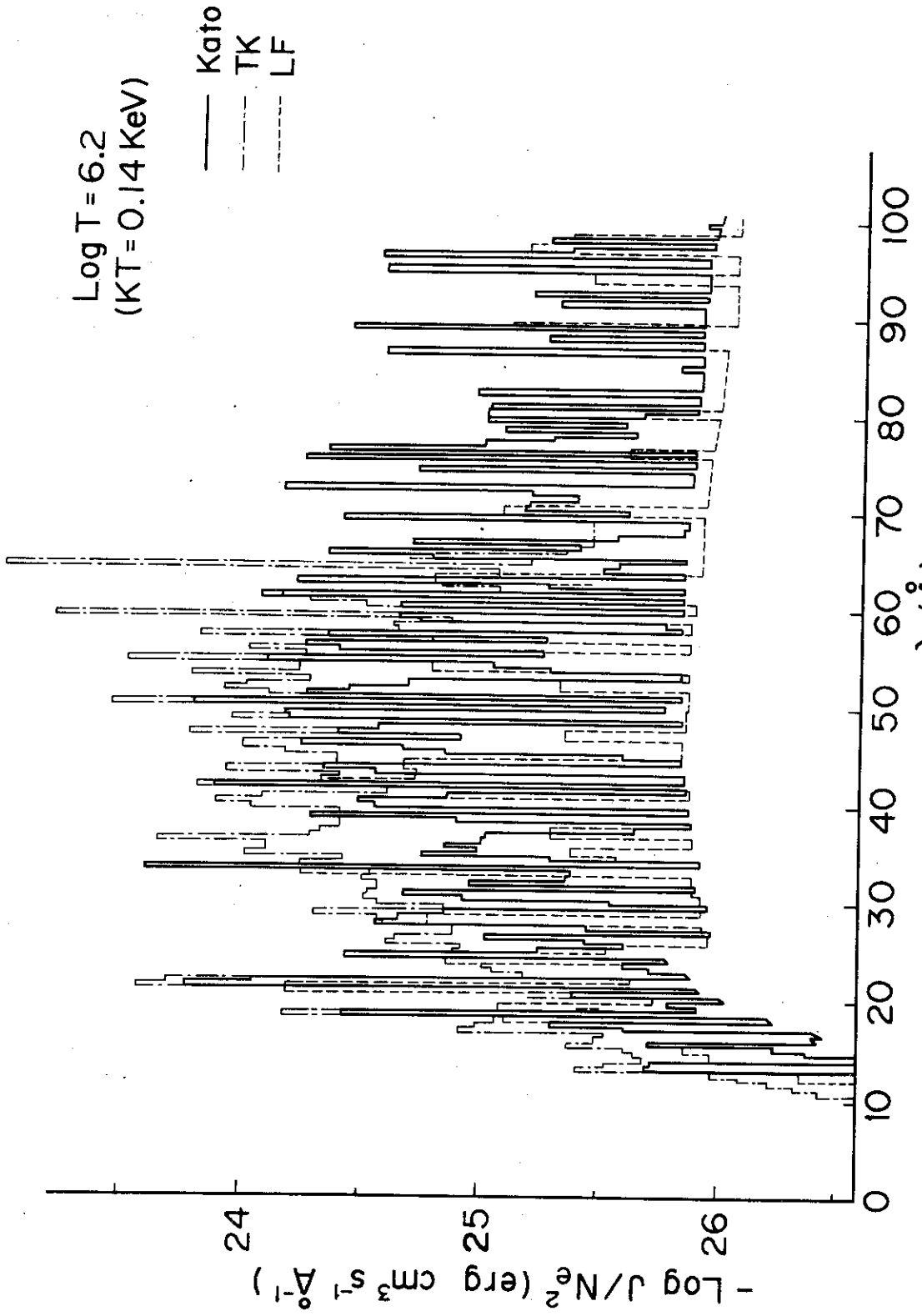
Log T = 6.2
(KT = 0.14 KeV)
Kato
TK
LF
- Log J/Ne2 (erg cm3 s-1 Å-1)
24
25
26
0
10
20
30
40
50
60
70
80
90
100
λ (Å)

Fig. 9

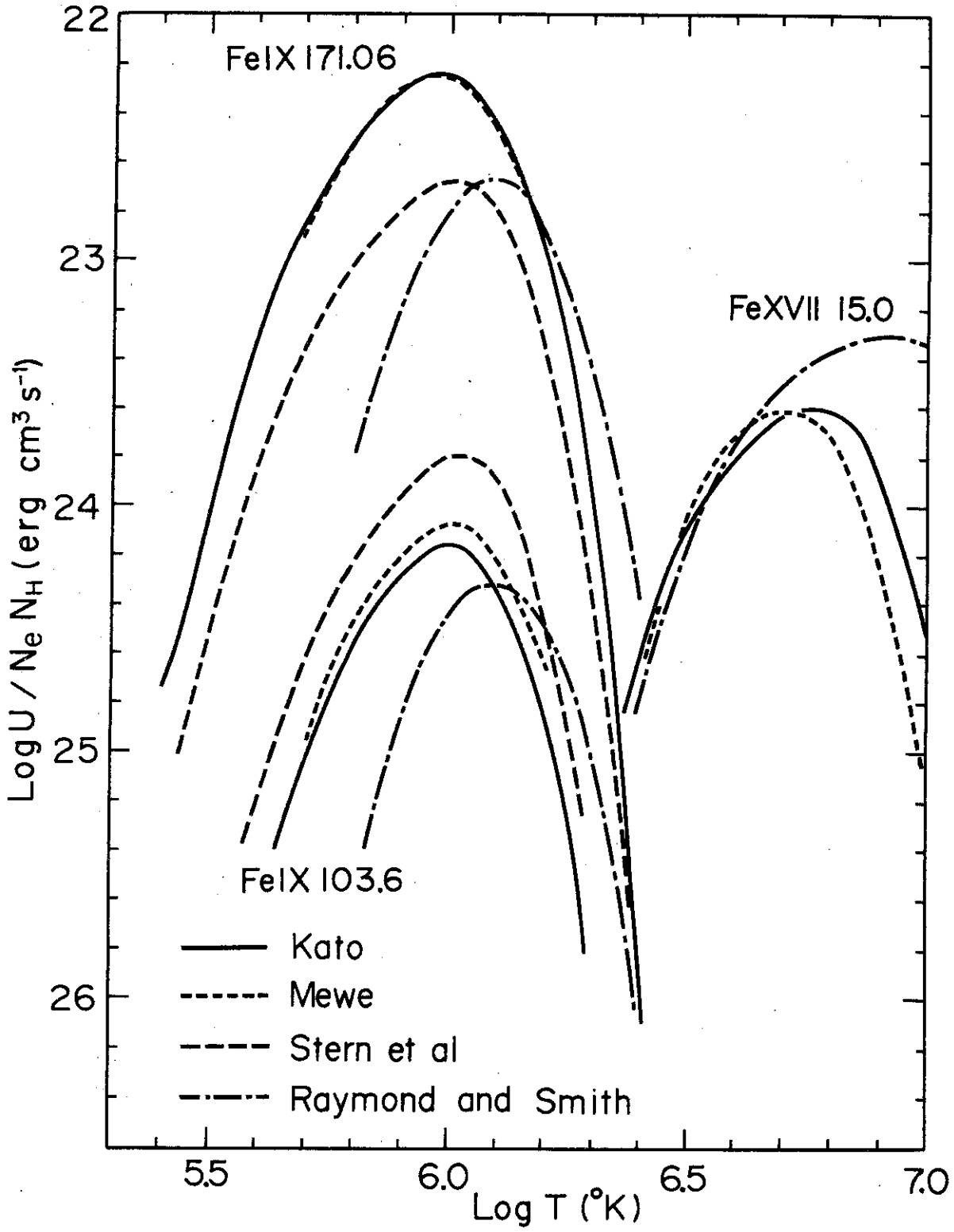
FeIX 171.06
FeXVII 15.0
FeIX 103.6
Kato
Mewe
Stern et al
Raymond and Smith
22
23
24
25
26
5.5
6.0
6.5
7.0
Log T (°K)
Log U / Ne NH (erg cm3 s-1)

Fig. 10

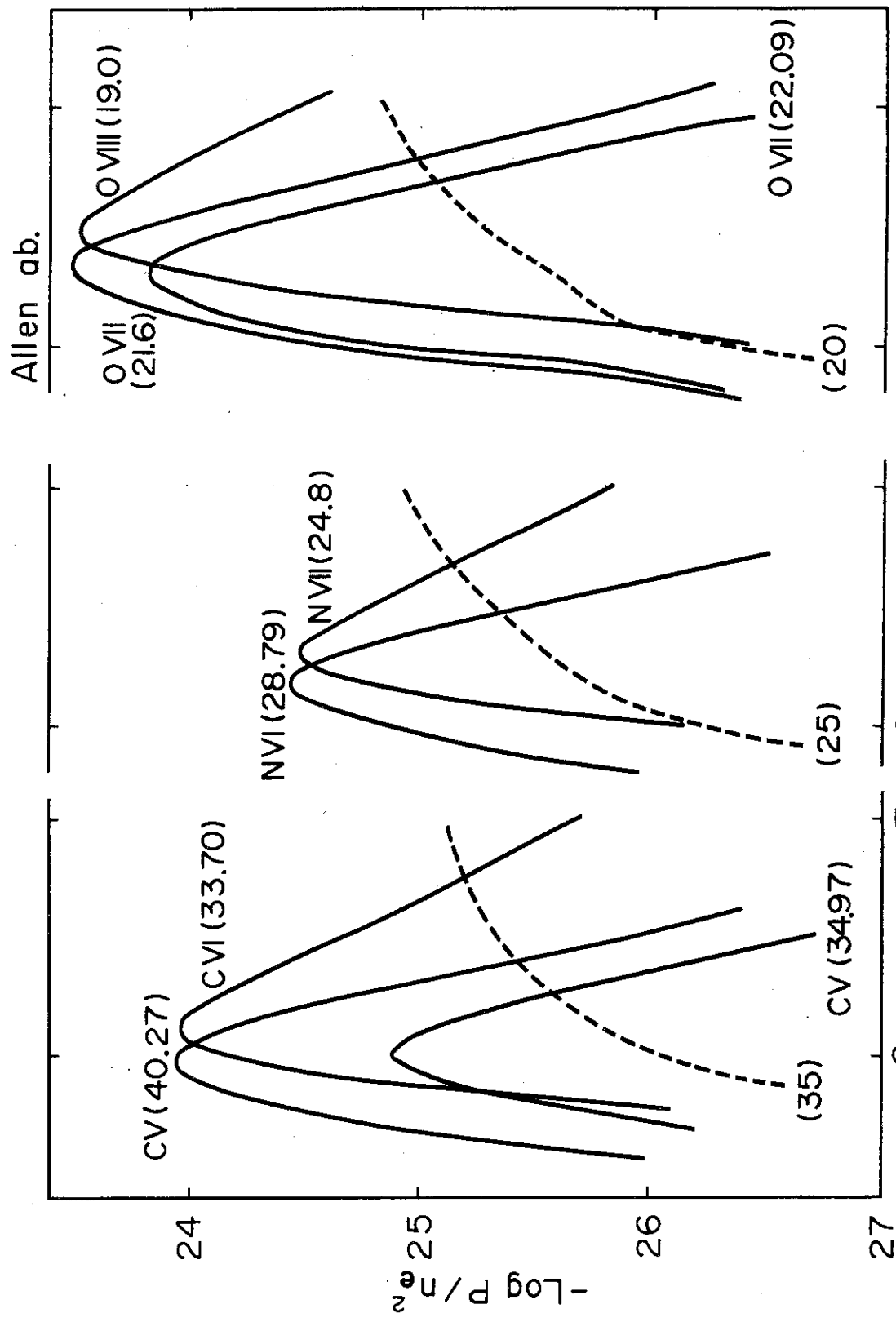
Allen ab.
O VIII (19.0)
O VII (21.6)
O VII (22.09)
(20)
NVI (28.79)
NVII (24.8)
(25)
CV (40.27)
CVI (33.70)
CV (34.97)
(35)
-Log P/n$_e^2$
Log T(°K)
24
25
26
27
6
7

Fig. 11 (a)

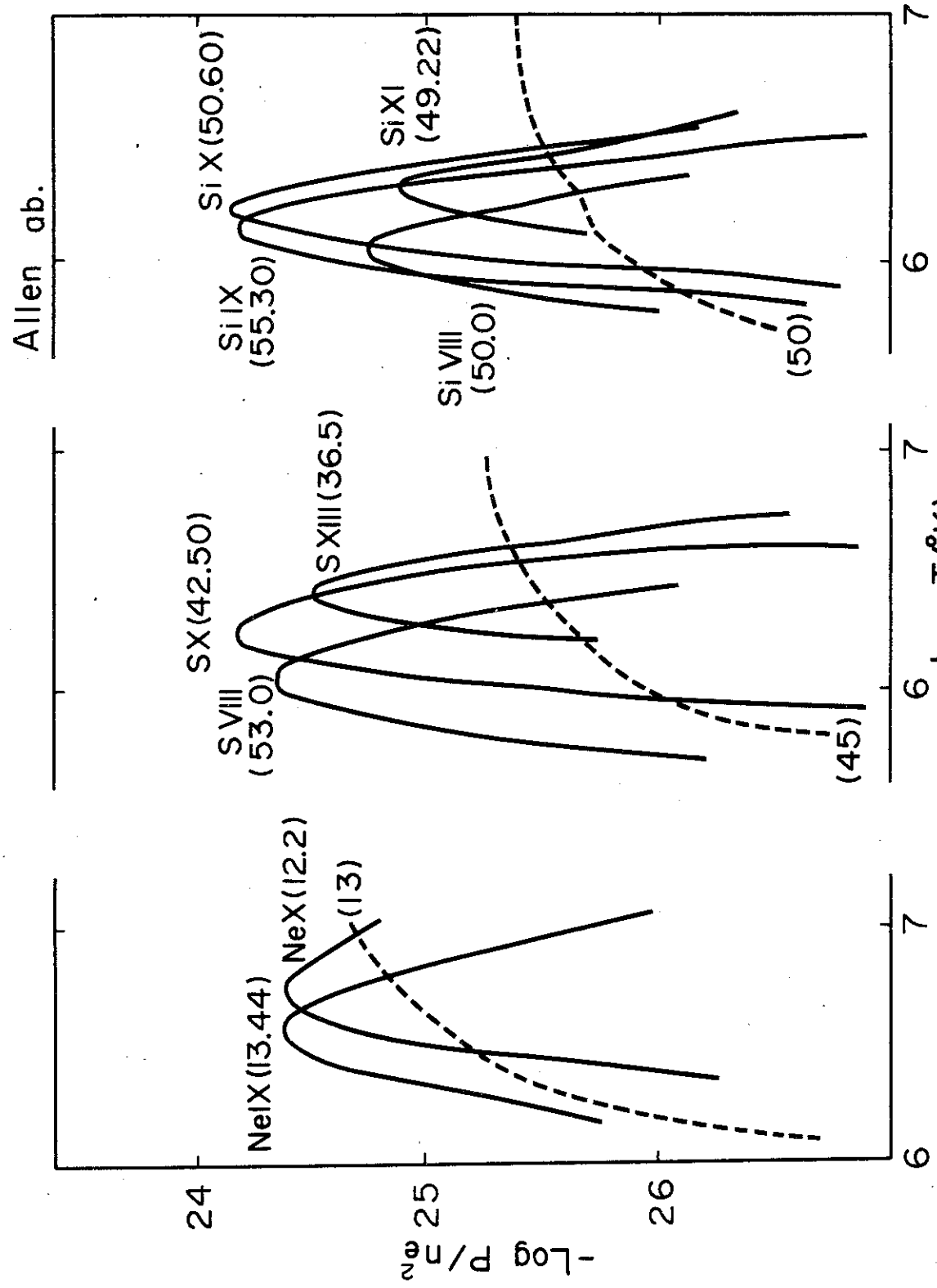
Allen ab.
Si X(50.60)
Si XI (49.22)
Si IX (55.30)
Si VIII (50.0)
(50)
SX(42.50)
SXIII(36.5)
SVIII (53.0)
(45)
NeIX(13.44)
NeX(12.2)
(13)
-Log P/n_e
Log T(°K)

Fig. 11(b)